International Journal of Greenhouse Gas Control 129 (2023) 103990

Contents lists available at ScienceDirect

International Journal of Greenhouse Gas Control

journal homepage: www.elsevier.com/locate/ijggc

Experimental investigation of multiple industrial wastes for carbon dioxide removal strategies

Liam A. Bullock [a,*], Jose-Luis Fernandez-Turiel [a], David Benavente [b]

[a] Geosciences Barcelona (GEO3BCN), CSIC, Lluís Solé i Sabarís, s/n, Barcelona 08028, Spain
[b] Department of Earth and Environmental Sciences, University of Alicante, Alicante 03690, Spain

ARTICLE INFO

Keywords:
Geochemical CDR
Co_2 removal
Industrial by-products
Mineral carbonation
Alkalinity generation
Dissolution rate

ABSTRACT

Industrial solid waste by-products are being increasingly employed for geochemical carbon dioxide removal (CDR) strategies due to their fine grain size, accessibility, and large annual production tonnages. Here, a range of such by-products has been tested experimentally for their reactivities with CO_2 and water. Sample solutions were monitored for 100 h for changes in chemistry, and solid samples were characterised pre- and post-experiment. Samples rich in Ca- and Mg-bearing minerals, such as dunite, kimberlite, and ilmenite mine tailings, as well as marble quarry cuttings, were key cation sources. Ni sulphide, fluorite and borax tailings, coal-fired power plant fly ashes, and red mud samples showed high dissolution rates. The highest reaction rates were often observed during the initial few hours, and compared well to rates determined for rocks typically targeted for CDR purposes, such as basalt and gabbro. Several samples also showed secondary carbonate precipitation, suggesting opportunities for the development of single-step CDR technologies. Overall, the results of this study indicate that several industrial by-products can provide sufficient cations at favourable dissolution rates for geochemical CDR purposes. Any on-site or near-site conditions for reaction acceleration such as heat, concentrated CO_2 or microbes, could further increase favourability for geochemical CDR opportunities.

1. Introduction

The necessity for carbon dioxide removal (CDR) from the atmosphere on the order of tens of gigatonnes (Gt) per year by 2100 (Intergovernmental Panel on Climate Change (IPCC), 2018, 2019; National Academies of Sciences, Engineering, and Medicine (NASEM) 2019; United Nations Environment Programme (UNEP) 2022) is a formidable challenge, requiring an urgent evaluation of different available CDR strategies. One emerging approach is through *ex-situ* geochemical CDR, such as targeted enhanced weathering, ocean alkalinity enhancement (OAE), and mineral carbonation approaches using industrial by-products (Bullock et al., 2021; 2022; Campbell et al., 2022; Declercq et al., 2023; Lu et al., 2023; Mervine et al., 2018; Paulo et al., 2021; Power et al., 2020; 2013a; 2014; 2013b; Pullin et al., 2019; Stubbs et al., 2022; Wilson et al., 2009a; 2014). The principle is to promote or accelerate natural chemical weathering through the utilisation of loose, excavated, or processed natural materials (e.g., basalt) or artificial materials (e.g., industrial wastes). This involves Ca-Mg-bearing minerals undergoing dissolution in a one-step reaction with CO_2 (and typically water) to form soluble bicarbonates, or a two-step reaction to form new carbonate minerals (summarised in Fig. 1). For example, reactions which may occur through reacting Ca-Mg minerals with CO_2 and water include:

Wollastonite (wo) weathering: $CaSiO_3$ (wo) + CO_2 + $2H_2O$ → $CaCO_3$ + H_4SiO_4 (1)

Olivine (forsterite, fo) weathering: Mg_2SiO_4 (fo) + $2CO_2$ + $2H_2O$ → $2MgCO_3$ + H_4SiO_4 (2)

The products are stored as cation-stabilised bicarbonate solution (alkalinity), achieving CDR, or precipitate from bicarbonate to form carbonate minerals:

Calcite (cal) precipitation: $Ca^{2+} + 2HCO_3^- \rightarrow CaCO_3$ (cal) + H_2O + CO_2 (Eq. 3)

Magnesite (mgs) precipitation: $Mg^{2+} + 2HCO_3^- \rightarrow MgCO_3$ (msg) + H_2O + CO_2 (Eq. 4)

Through the precipitation of carbonates, some CO_2 is returned to the atmosphere. Both the weathering and precipitation reactions can net

* Corresponding author.
E-mail address: lbullock@geo3bcn.csic.es (L.A. Bullock).

https://doi.org/10.1016/j.ijggc.2023.103990
Received 8 June 2023; Received in revised form 18 August 2023; Accepted 29 September 2023
Available online 5 October 2023
1750-5836/© 2023 The Authors. Published by Elsevier Ltd. This is an open access article under the CC BY-NC-ND license (http://creativecommons.org/licenses/by-nc-nd/4.0/).

consume CO_2 (except for weathering and subsequent re-carbonation of carbonates), storing it safely for hundreds of thousands of years or longer. However, this slow process takes several hundred years or more to occur. One key strategy for geochemical CDR is to accelerate the weathering (dissolution) and precipitation processes in such a way that significant amounts of CO_2 are removed from the atmosphere on human timescales (e.g., up to tens of years, or faster). Approaches to achieving geochemical CDR include subsurface *in-situ* processes for mineral carbonation within suitable bedrock units (requiring concentrated CO_2 either through direct air capture (DAC) or carbon capture technologies), and *ex-situ* alkalinity generation and mineral carbonation of suitable loose or crushed materials (Fig. 1) (Campbell et al., 2022).

Several industrial waste by-products have been studied for their *ex-situ* geochemical CDR potential based on several advantages over natural systems (Bullock et al., 2023a; Harrison et al., 2013; Huijgen et al., 2005; McCutcheon et al., 2015, 2016; Power et al., 2020; 2016; 2013a; 2014; Renforth et al., 2011; Renforth, 2012; Wilson et al., 2009a,b). This feature is particularly true for volumetrically-abundant and fine-grained silicate-rich mine tailings, with potentially up to 17 Gt of material produced per year globally (Bullock et al., 2021) and ten- to hundred-fold more historic tailings stockpiled on mine sites. Of the global annually generated silicate-hosted tailings, potentially up to 2 Gt may be identified as materials of high reactivity with CO_2 and of high CDR potential (Bullock et al., 2022). These materials include reactive minerals derived from asbestos and talc-hosting serpentinite-hosted deposits (Dichicco et al., 2015; McCutcheon et al., 2016; 2017; Power et al., 2013b; Paulo et al., 2021; Wang and Maroto-Valer, 2011), Ni-rich sulphide deposits (Assima et al., 2014; Kandji et al., 2017; Power et al., 2020; Wilson et al., 2014), kimberlite diamond mines (Bullock et al., 2023b; Mervine et al., 2018; Paulo et al., 2021; Wilson et al., 2009b; Zeyen et al., 2022), and olivine and serpentine-rich dunites mined as refractory minerals (Bullock et al., 2023a; Hangx and Spiers, 2009; Kremer et al., 2019; Kremer and Wotruba, 2020; Renforth et al., 2015; Schuiling and de Boer, 2011; ten Berge et al., 2012).

Similarly, non-silicate hosted tailings have also been identified for their geochemical CDR potential, including limestone-hosted aggregates and metal deposits (Foteinis et al., 2022; Renforth et al., 2013, 2022), and Al-rich red muds (Bonenfant et al., 2008; Renforth, 2019), while borax-rich deposits may act to catalyse CO_2 absorption in solution (Guo et al., 2011). A major benefit for tailings and similar alkaline industrial wastes, such as glassy slags and combustion fly ashes (Campbell et al., 2022; Ebrahimi et al., 2018; Huijgen et al., 2005; Mustafa et al., 2020; Rausis et al., 2021; Reddy et al., 2009; Renforth, 2012; 2019; Reynolds et al., 2014; Wang et al., 2022), over natural rocks for CDR purposes is that they are typically available in fine grain sizes as part of the conventional industrial process, so no additional energy requirements are needed to achieve these favourable grain sizes. Finer grains result in higher, fresher reactive surface areas for reactions with CO_2 to take place (Bodénan et al., 2014; Bullock et al., 2021; Campbell et al., 2022; Hitch et al., 2010; Li et al., 2018; McCutcheon et al., 2016; Pronost et al., 2011; Renforth, 2019; Vance et al., 2009; Vogeli et al., 2011). Furthermore, materials such as fly ashes and slags may be produced proximal to a CO_2 emission point source (e.g., coal-fired power plants, metal refineries) that could be utilised for CDR purposes on-site (Wang et al., 2019).

The academic and industrial attention being paid to such physically-favourable industrial wastes highlights the high potential for CO_2-water-solid material reactions for large-scale geochemical CDR purposes, either hosted on-site (e.g., reactor-based schemes; (Xing et al., 2022)) or in other *ex-situ* settings (e.g., field-based schemes; Beerling et al., 2020). However, critical uncertainties remain regarding which by-product materials are appropriately reactive and at what dissolution rates (W_r), requiring further attention. While mafic and ultramafic-rock derived alkaline industrial wastes are generally considered the best candidates for geochemical CDR purposes, more studies are required to further understand their reactions. Furthermore, rigorous experimental studies on other industrial materials, such as Al-associated red muds, borate deposits, lime-treated tailings, SO_2-processing products, and Cu-related tailings, highlighted for their possible CDR potential (e.g.,

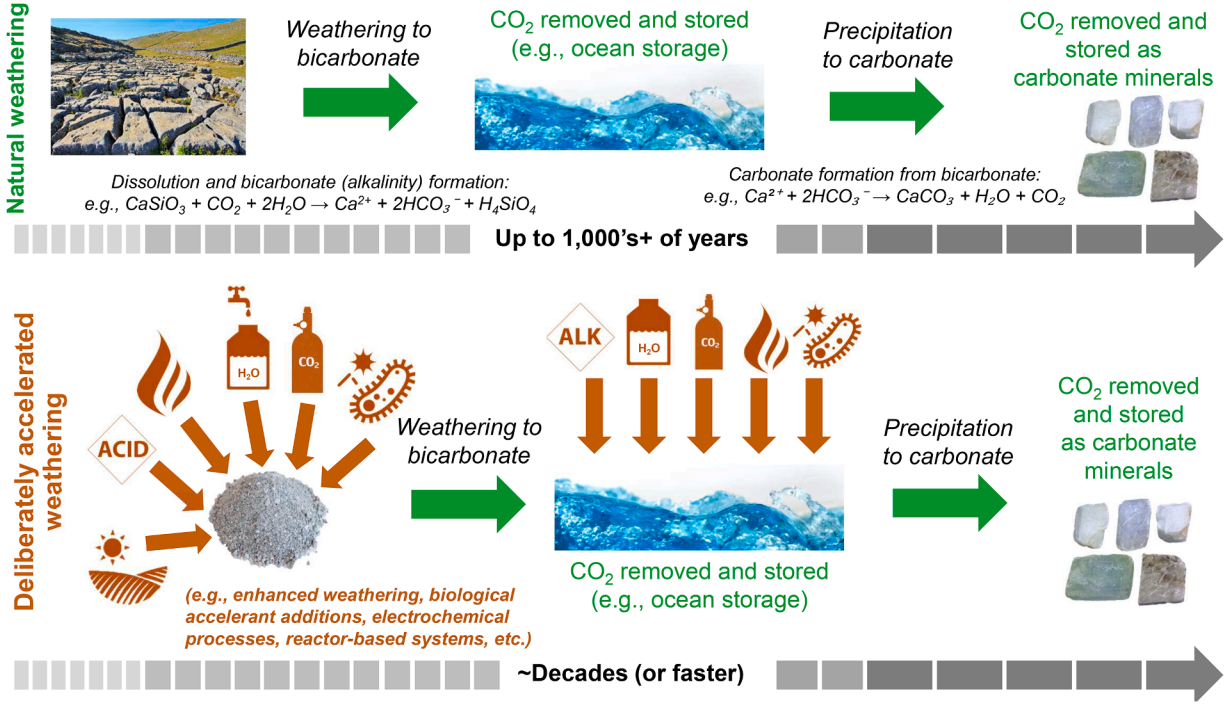

Fig. 1. Summary of principle reactions and processes involved in natural and deliberately accelerated weathering to produce bicarbonate alkalinity and/or carbonate minerals to achieve CDR. The addition of CO_2 to water (in the atmosphere or by direct injection) leads to formation of carbonic acid (H_2CO_3), dissociating into hydrogen ions (H^+) and bicarbonate ions (HCO_3^-), acting to decrease pH, trigger disequilibrium between mineral and water, and leading to mineral dissolution. The additional Ca^{2+} or Mg^{2+} in solution and presence of hydroxide ions (OH^-) increases pH, promoting the formation of carbonate ions (CO_3^{2-}), and invoking Ca-carbonate (e.g., calcite; $CaCO_3$) or Mg-carbonate (e.g., magnesite; $MgCO_3$) precipitation from solution.

Bullock et al., 2021, 2022; Guo et al., 2011; Jones et al., 2006; Renforth, 2012; 2019; Srivastava et al., 2022), are generally lacking.

This study investigates the ambient-temperature reactivity of a wide range of industrial wastes with CO_2 and water, with the primary goal of identifying viable cation sources at promising W_r for possible CDR strategies. The sample set, derived from industrial sites distributed globally, includes materials generally considered to be chemically and mineralogically favourable for CDR (e.g., diamond kimberlite, dunite, and Ni sulphide tailings), materials that may be promising (e.g., ilmenite tailings, Al red muds, borax tailings) and materials of unknown or minor promise (e.g., lime-treated and untreated Cu tailings, SO_2-processing products, fly ashes, and Cu slags). The aim is to identify the materials that show suitable potential for CO_2-water-solid material reactions for targeted future CDR methods and upscaled and accelerated removal strategies. This study also investigates the post-experimental changes to physical, chemical, and mineralogical (observed and predicted) properties of by-product samples to assess better the overall geochemical CDR potential and different CDR strategies (e.g., alkalinity production vs. carbonate precipitation) that could be targeted. A better understanding of reaction kinetics across a broader range of industrial wastes will aid future projects in confirming or re-evaluating the viability of materials for various CDR schemes. This will also help identify opportunities for upscaled pilot schemes, incorporating advanced geochemical CDR methods to expedite reaction kinetics.

2. Materials and methods

2.1. Materials

Twenty-one industrial processing residual materials related to global site operations were selected for this study. Samples include tailings derived from mine operations targeting diamond-hosting kimberlites, dunites, borax, copper (Cu), ilmenite, fluorite, and Ni sulphides, as well as Al-bauxite-related red muds, Cu refinery slags, products from sulphur dioxide (SO_2) processing, carbonate marble fine cuttings, and coal-fired power plant fly ashes (Table 1). Changes to water chemistry through reactions with CO_2 and powdered material samples were monitored throughout the experiment. These include changes to pH, alkalinity indicators, silica content, and cation content (labile cations leaching from solid samples), predominantly Ca^{2+} and Mg^{2+}, required for reactions with CO_2 (available as dissolved inorganic carbon, DIC) to produce bicarbonate (HCO_3^-, stabilised by cations) and carbonate (CO_3^{2-}, stabilised by cations) ions.

Table 1
Industrial by-product samples utilised in this study.

Sample code	General sample description	Locality
Diamond kimberlite mine tailings		
DFT	Diamond mine kimberlite fine tailings	Northwest Territories, Canada
DK	Diamond mine kimberlite fine tailings	Northwest Territories, Canada
ACT	Diamond mine kimberlite coarse tailings	Western Australia
Dunite mine tailings		
DUL	Dunite mine fine tailings (<100 μm)	Galicia, Spain
DUN	Dunite mine coarse material (0–3 mm)	Galicia, Spain
Al-red mud mine tailings		
GRM	Aluminium mine red mud tailings	Northern Territory, Australia
NRMS	Aluminium mine seawater neutralised red mud tailings	Queensland, Australia
Borax mine tailings		
BAP1	Boron mine tailings	California, United States
BAP2	Boron mine tailings	California, United States
BRP	Boron mine tailings	California, United States
Cu mine tailings		
RTKC	Copper mine tailings	Utah, United States
SDS	Copper mine tailings	Unknown
A-ESC	Copper mine mixed dump materials	Andalucía, Spain
A-EP	Copper mine lime-treated tailings	Andalucía, Spain
Cu slag material		
ACS	Copper refinery slags	Andalucía, Spain
Ilmenite mine tailings		
SCDS	Ilmenite mine tailings	Quebec, Canada
SO_2 processing plant by-products		
SSO2	Mud product from SO_2 processing	Victoria, Australia
Marble fine cuttings		
MAR	Marble quarry fine waste cuttings	Alicante, Spain
Fluorite mine tailings		
MFA	Fluorite mine tailings	Asturias, Spain
Ni sulphide mine tailings		
WCN	Nickel sulphide mine tailings	Ontario, Canada
Coal-fired power plant fly ash		
FA	Coal-fired power plant-derived fly ash	León, Spain

2.2. Sample characterisation

2.2.1. Scanning electron microscopy

Pre-experimental textural and mineralogical characteristics were examined using a Jeol IT500HR/LA electron microscope (SEM), equipped with a Raith Elphy Quantum X-ray detector for energy dispersive X-ray spectroscopic (EDS) microanalysis, at the Research Support Services, University of Alicante.

2.2.2. X-Ray diffraction

Mineralogical characterisation, including quantitative modal mineral abundances, was performed by X-ray diffraction (XRD) analysis. Samples were analysed using a Bruker D8-A25 diffractometer instrumentation at GEO3BCN, CSIC. Fine powdered (<70 μm) samples were placed on a flat disk sample holder, compressed, and scanned (Cu K-α1 radiation, λ=1.5406 Å, at 40 kV and 40 mA), collecting data between 4° and 60° of 2θ, with a scan step of 0.05° and a contact time of 5 s. Diffractogram evaluations were carried out using DIFFRAC software. Moreover, XRD data were interpreted using the XPowder software package, which allows the calculation of amorphous content. It considers that amorphous absorption contributes to the full-profile background, representing a percentage of amorphous phases in the sample (Benavente et al., 2020; Martín Ramos, 2004; Pla et al., 2021; Sanjuán et al., 2019).

2.2.3. Major and trace element geochemistry

Whole rock composition was determined by a combination of X-ray fluorescence (XRF) spectrometry, loss on ignition (LOI), and inductively coupled plasma-mass spectrometry (ICP-MS), performed at ALS Geochemistry Services (Seville, Spain; ALS code CCP-PKG03). Certified reference materials (CRM) analysis results were within the expected target range for each analyte. Duplicate analyses produced values within the acceptable range for laboratory duplicates, with an average relative per cent difference of ±5 %. Total carbon (TC), total inorganic carbon (TIC), and total organic carbon (TOC) contents of materials were measured using a LECO SC-144DR elemental analyser at the University of Leeds. Analyses were run concurrently with LECO instrumental standards (LECO part No. 502–062 Lot 1018, 0.924 % C), and the repeatability, based on repeats of standards and blanks, was typically within 1 %, with a maximum relative error of ~3 %.

2.2.4. Grain size distribution

The experiments aimed to use a sample size range that may reflect a typical average particle size present for a range of waste types on an industrial site. Representative cited particle sizes, where values are presented as mean particle sizes or d90 values, typically range from ~75 μm (e.g., Amponsah-Dacosta, 2017; Rackley, 2017; Swami et al., 2007) up to 250 μm (e.g., Das, 2015), with several values between 75 and 250 μm also cited (e.g., Rodríguez et al., 1998; European Commission, 2009; Hu et al., 2017; Kursun et al., 2017; Schulz et al., 2017). Slag samples may be coarser, up to 2 mm, and fly ash samples may be finer than 64

μm, though both can show wide distributions. The aim was also to closely reflect at least some of the inherent particle size variability in tailings ponds and similar settings, as well as the probable size distribution which would be considered present in any implemented large-scale geochemical CDR system. This means that some finer and coarser material would also be present (any additional extensive high-resolution screening of fines and slightly coarser material specifically for CDR purposes would likely be costly and time consuming in such a system). However, the aim was also to be able to compare samples to each other, meaning a close average grain size and grain size distribution would also be required. For these reasons, all samples were crushed, homogenised and dry-sieved once using a sieve shaker (up to 20 min at a high shake power setting) to achieve a general majority size range of 63–250 μm.

Pre-experimental particle size distributions were determined using a Malvern Mastersizer 3000 laser diffraction particle size analyser at GEO3BCN, CSIC. The analyser, equipped with a laser diffractometer (ultrasonic water disaggregation: Hydro MU system; absorption: 0.1; refractive index: 1.52; measurement time: 20 s; obscuration: 10–20 %; pump speed: 2500 rpm, five measures; material amount per run: ~1 g; measurement range: 0.1 to 1000 μm), provides the particle size abundance as the average volume percentage of equivalent spherical diameter, measured over five runs. The analyser also gives statistical particle information such as specific geometric surface area (G-SSA) and d10, d50 and d90 values (% of particles smaller than each size bracket).

2.2.5. Specific surface area

When a reaction is surface controlled, measured overall reaction rates are directly proportional to the surface area involved and thus must be normalised by a surface area term to obtain the rate constant. Two main methods can calculate surface area measurements: G-SSA calculated from grain diameter, and specific surface area determined by the Brunauer-Emmett-Teller or BET method (BET-SSA) (Brunauer et al., 1938). Generally, BET measurements are used in most studies due to their robustness compared to geometric measurements (Liittge and Arvidson, 2008), though both methods show advantages and limitations for W_r determination. BET considers surface roughness, such as pits and cracks, giving a higher measurement. The specific surface areas of samples were measured by the gravimetric nitrogen BET method at the University of Barcelona (Micromeritics ASAP 2000 Micropore Analyser) and the University of Alicante (Quantachrome Instruments Autosorb-6 equipment). Samples were degassed for 24 h at approximately 140 °C prior to adsorption isotherm determination, with nitrogen adsorption isotherms obtained at liquid nitrogen temperature. Values for G-SSA were also co-determined by Malvern Mastersizer during grain size distribution analysis.

2.3. Experimental procedure

All samples were tested for their reactivity with CO_2 and water under controlled conditions using a benchtop experimental open system setup at GEO3BCN, CSIC (Fig. 2). The setup utilised bottled samples, tested for 100 h over three runs and three weeks (three runs of seven samples, with a blank control bottle for each run, bottled placed in a row and connected by the gas tube). The 500 ml bottles were initially washed to ensure no contamination was present. The cleaned bottles were filled with 500 ml of purified water of 18.2 MΩ/cm type Milli-Q Plus. Bottles were placed on multi-platform shaker plates to ensure some sample mobilisation during the experiment, operating at a near-constant rate of 125 rpm. At the onset of the experiments, ~10 g of dry sample was added to each bottle, fitted with a CO_2 gas line, as well as an overpressure release valve and valve extraction point, allowing for regular fluid sample extractions during the experiment. The CO_2 flow was running during the experiment at a rate of ~1.5 standard cubic feet per hour. The experiment commenced following a ~48-hour CO_2-fluid saturation-equilibration period before adding the samples. Following equilibration, an initial pH measurement was taken for each bottle. The samples were then added, with one bottle remaining blank (Milli-Q water) to account for the effect of CO_2 fluctuations during the experiment. Solution sampling began immediately following the addition of solid samples. The solution pH and the specific conductivity (SC) were monitored and recorded throughout the experimental duration. When pH fluctuations stabilised after 100 h, sampling and the experiment were concluded. As well as regular sampling for cation content, a visual (colour change-based) indicator of carbonate hardness and alkalinity was determined regularly *in-situ* by volumetric titration using VISOCOLOR® HE Carbonate Hardness C 20 kit (accuracy ± 0.2 mmol/L H^+). Carbonate hardness is a measure of carbonates and bicarbonates present in water. The method requires extraction of 5 ml of solution per sample point, meaning sampling was restricted to 1–2 times per day to avoid rapid depletion of solution across the experimental time. The *in-situ* measurement method visually evaluates alkalinity using indicator and titration solutions and changes in colour to estimate carbonate hardness (m-value) and partial alkalinity (p-value), converted to major element

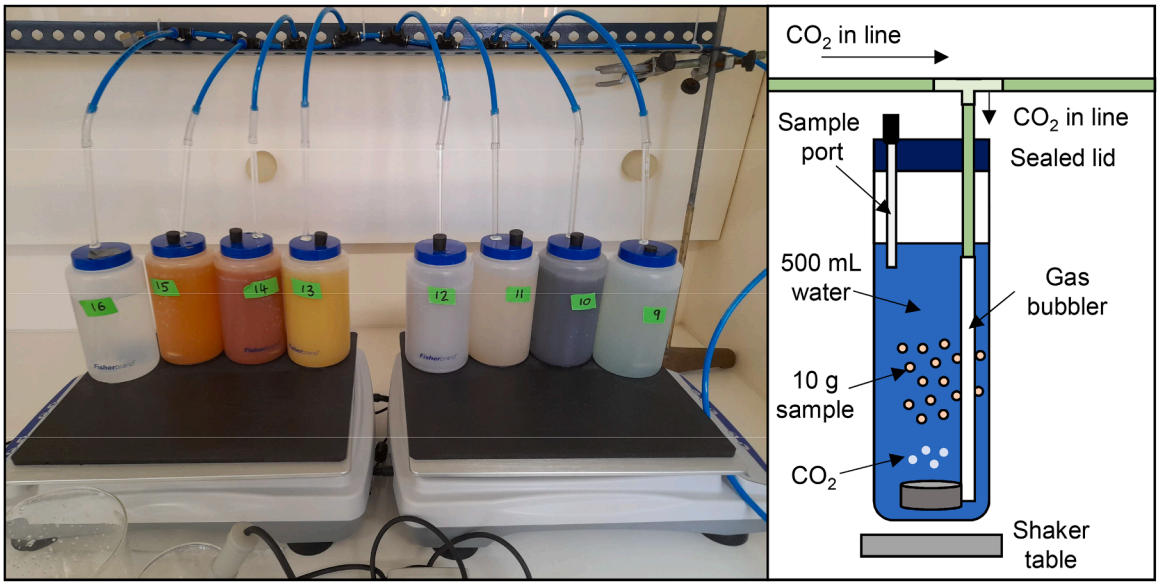

Fig. 2. Experimental setup, utilising bottles containing 10 g sample, 500 ml water, and CO_2 gas on the shaker tables.

oxide (e.g., Ca, Mg, Na, Fe), carbonate, and H^+ concentrations.

2.4. Post-experimental results

Remaining solid samples were removed from bottles within 24 h of the experiment finishing, with no additional shaking or CO_2 gas input to limit post-experimental effects on both the solid and fluid properties. Following drying and sieving, solid sample weights were measured post-experiment to indicate sample loss by mineral dissolution. Post-experimental XRD, BET-SSA measurements and TC/TIC/TOC concentrations were also determined on sample materials, following drying, using the same methods outlined above.

Cation W_r was calculated for Ca, Si, and Mg using Eq. (5) below:

$$r_x = log\left(\frac{\Delta X \times M_w}{A_{BET} \times M_r \times t}\right) \quad (5)$$

where r_x is the W_r of element x shown as log x (mol/cm^2/s), ΔX is the aqueous concentration of element x (converted to mol/kg), M_w is the water mass at each sample point (kg), A_{BET} is the BET-derived SSA of rock powders before the experiment (converted to cm^2/kg), M_r is the original material mass (kg), and t is the elapsed time in seconds from $t = 0$ (see also (Marieni et al., 2020)).

In this study, in the absence of adequate time to precipitate demonstrable amounts of secondary carbonate minerals (and means to measure their occurrence in such probable low abundances, e.g., below XRD detection limits), the geochemical modelling program PHREEQC (version 3.7.0; (Parkhurst and Appelo, 2013), with MINTEQ database) was used to predict the possible precipitating phases that may result from reactions of each sample with pure water, at conditions similar to those of the experimental setup (temperature of 25 °C, starting pH of 4, with fixed pressure of a CO_2-rich gas), with sufficient time to react 100 % of available elements in the solution and material. For each sample run, equilibrated Ca- and Mg-bearing phases (cation sources for possible carbonate precipitates) of the starting materials were assumed based on the modal XRD, where present.

3. Characterisation results

3.1. Pre-experimental sample characterisation

The physical and mineralogical properties of the samples selected for this study are shown in Table 2, Fig. 3 and Supplementary Material (SM) Table I. The geochemical characteristics are shown in Table 3 and SM Table II.

3.2. Grain size distribution and surface area

As a result of the initial screening and dry sieving process, the d90 value across all samples ranges from 46 (sample DUL) to 346 μm (ACS glassy slag sample), averaging 155 μm. Most samples show polydisperse distributions (monodisperse distributions – MFA and ACS), with no particles identified below a size of ~0.2 μm. Few samples show modal volumes greater than 1 % for particles below ~1 μm (SM Table I). The largest recognised grain size was at a size classification of ~1002 μm (samples BRP, BAP2 and WCN), with few particles identified as larger than ~355 μm across all samples. Some distributions generally trend towards coarser grain sizes and monomodal distributions, with the highest modal values greater than 100 μm (e.g., SDS, GRM, ACT, ACS, and MFA), while several samples show a bimodal distribution. G-SSA values range across deposits from 0.12 m^2/g (sample ACS) to 1.51 m^2/g (sample BAP1), averaging 0.85 m^2/g across all samples (SM Table I).

3.3. Sample mineralogy

The modal mineralogy of samples was determined by XRD and

Table 2
Pre-experimental physical and mineralogical characteristics of samples. For modal mineralogy of glassy samples (e.g., ACS and FA),% represents proportion of total crystalline phases identified, while amorphous content represents glassy proportion of total sample material.

Sample	Grain size percentiles (μm)			BET-SSA (m^2/g)	Modal mineralogy, excluding amorphous content (XRD)	Amorphous content (%)
	d10	d50	d90			
Diamond kimberlite mine tailings						
DFT	2.0	14.0	99.7	19.5	Muscovite (22.2 %), quartz (21.3 %), forsterite (15.8 %), notronite (11.3 %), calcite (10.3 %), microcline (9.1 %), albite (4.6 %), dolomite (3.4 %), clinochlore (2.0 %)	30.4
DK	2.0	12.2	102.6	34.8	Forsterite (22.4 %), microcline (19.3 %), quartz (16.3 %), albite (15.3 %), muscovite (11.0 %), calcite (6.8 %), nontronite (2.8 %), clinochlore (2.5 %), dolomite (2.1 %), clinochrysotile (1.5 %)	32.0
ACT	4.4	84.4	257.7	2.8	Quartz (78.5 %), clinochlore (8.8 %), microcline (7.1 %), muscovite (3.5 %), calcite (1.4 %), talc (0.7 %)	3.8
Dunite mine tailings						
DUL	2.2	13.2	46.2	18.4	Lizardite (43.8 %), clinchlore (41.9 %), dolomite (7.4 %), tremolite (6.9 %)	25.1
DUN	1.6	23.2	114.2	10.0	Lizardite (56.4 %), enstatite (15.0 %), tremolite (12.9 %), forsterite (8.9 %), clinochlore (6.8 %)	44.2
Al-red mud mine tailings						
GRM	8.5	71.1	189.5	24.9	Gibbsite (41.6 %), quartz (19.3 %), haematite (17.8 %), anatase (5.2 %), calcite (5.1 %), kaolinite (4.3 %), muscovite (2.1 %), rutile (1.5 %)	50.0
NRMS	1.5	26.5	118.9	33.1	Sodalite (43.7 %), haematite (15.8 %), halite (10.9 %), anatase (7.4 %), boehmite (6.9 %), calcite (5.1 %), quartz (4.6 %), gibbsite (3.5 %), magnetite (1.1 %), rutile (1.0 %)	50.0
Borax mine tailings						
BAP1	1.4	11.6	48.6	2.5	Thenardite (81.3 %), sassolite (7.8 %), albite (4.1 %), microcline (3.9 %), quartz (1.7 %), muscovite (0.6 %), halite (0.6 %), rhomboclase (0.1 %)	15.4
BAP2	1.9	14.5	96.9	2.1	Borax (48.9 %), thenardite (21.7	14.6

(continued on next page)

Table 2 (*continued*)

Sample	Grain size percentiles (μm)			BET-SSA (m^2/g)	Modal mineralogy, excluding amorphous content (XRD)	Amorphous content (%)
	d10	d50	d90			
					%), tincalconite (14.8 %), ulexite (11.1 %) clinochlore (1.4 %), albite (1.0 %), microcline (0.9 %), quartz (0.1 %)	
BRP	6.4	81.7	282.1	0.8	Tincalconite (92.0 %), borax (6.7 %), quartz (1.3 %)	14.3
Cu mine tailings						
RTKC	1.3	14.9	68.8	17.3	Quartz (62.2 %), jarosite (11.2 %), sanidine (10.6 %), gypsum (9.8 %), muscovite (3.7 %), crocidolite (1.2 %), montmorillonite (0.7 %), nontronite (0.5 %)	12.5
SDS	43.6	107.1	203.8	1.4	Quartz (90.1 %), microcline (4.9 %), illite (4.7 %), pyrite (0.3 %)	3.2
A-ESC	2.4	28.2	212.8	3.1	Quartz (82.5 %), clinochlore (6.1 %), muscovite (5.7 %), jarosite (2.6 %), goethite (2.2 %), kaolinite (1.0 %)	9.6
A-EP	2.2	30.2	223.2	2.4	Quartz (54.7 %), clinochlore (38.8 %), siderite (2.4 %), muscovite (2.1 %), pyrite (2.1 %)	13.0
Cu slag material						
ACS	25.8	155.3	346.6	0.1	Maghemite (44.7 %), iscorite (27.9 %), fayalite (27.4 %)	50.0
Ilmenite mine tailings						
SCDS	6.0	20.7	97.8	9.7	Hannebachite (38.5 %), portlandite (23.2 %), thaumasite (20.9 %), calcite (15.5 %), phlogopite (2.0 %)	38.8
SO_2 processing plant by-products						
SSO2	1.4	33.7	145.7	9.3	Anorthite (44.0 %), ilmenite (17.8 %), albite (13.2 %), muscovite (9.8 %), haematite (7.3 %), rutile (4.5 %), clinochlore (3.5 %)	44.2
Marble fine cuttings						
MAR	6.9	34.1	215.2	3.3	Calcite (69.3 %), dolomite (30.5 %), quartz (0.3 %)	5.7
Fluorite mine tailings						
MFA	16.5	90.2	214.1	1.3	Quartz (70.0 %), fluorite (14.9 %), calcite (10.1 %), dolomite (3.7 %), illite (0.7 %), pyrite (0.5 %)	3.5
Ni sulphide mine tailings						
WCN	3.6	18.0	46.6	4.1	Lizardite (51.3 %), clinochlore (45.4 %), tremolite (3.2 %)	10.4
Power plant fly ash						
FA	4.0	43.3	120.9	1.9	Mullite (56.0 %), quartz (44.0 %)	50.0

verified by SEM-EDS. Of particular interest were phases that bear Ca, Mg, Na, and K (Fig. 3a-c), which may act to produce alkalinity (Kheshgi, 1995; Palandri and Kharaka, 2005), as well as phases rich in elements that are unlikely to react, which will hinder alkalinity production or promote acidity (e.g., Si, Mn, Al, Fe, B, S, P, N) (Fig. 3d-F). Minerals of interest for alkalinity and carbonate production are Mg- and Ca-bearing silicates, oxides, and hydroxides, as well as Na- and K-bearing phases. Carbonate minerals are also of interest due to their ability to generate alkalinity, but any subsequent carbonate precipitation that follows directly from carbonate dissolution would result in no net CO_2 uptake.

Tailings samples derived from dunite and Ni sulphide processing operations are comprised entirely of minerals that may react to produce bicarbonates and carbonates. In particular, the presence of forsterite (up to ~100 μm in length), lizardite (~50–100 μm), tremolite (~100 μm), chlorite (~100 μm), and enstatite (~120 μm) are promising for CO_2-water-mineral reactivity. The dunite samples also contain minor dolomite, and amorphous content of up to 44 % (similarly high amorphous content also noted in other studies; (Baragaño et al., 2019; Caballero et al., 2009)). Kimberlite-derived samples show similarly high potential, mainly due to the presence of forsterite, but also sporadic brucite phases (up to ~10 μm, identified by SEM-EDS, Fig. 3a), saponite, a smectite group mineral which contains Ca-Mg-Fe and may show some CDR potential (Cygan et al., 2012; Michels et al., 2015; Zeyen et al., 2022), and amorphous material (up to 30 %). Portlandite, a highly reactive Ca-hydroxide mineral and the Ca analogue of brucite was identified in ilmenite tailings. Calcite, thaumasite (Ca-silicate), and phlogopite (Mg-mica) are also present in ilmenite mine tailings. The presence of Na-rich minerals such as sodalite in red muds may also provide some CDR potential. Crocidolite, a fibrous Na-rich asbestiform amphibole, was also identified in one Cu tailings-derived sample (RTKC). This sample also contains sanidine and muscovite. Sample MAR, derived from marble fines, is almost entirely composed of carbonate minerals (calcite and dolomite).

Samples with high abundances of quartz (or other SiO_2 phases) and Al, Fe, and Ti-rich minerals (e.g., anatase, boehmite, gibbsite, goethite, haematite, and ilmenite) are unlikely to be favourable for CDR purposes. All Cu tailings samples show high quartz contents, with minor clays, Fe-oxides, and hydroxides phases also evident. Monazite, a phosphate mineral, was also identified in sample DFT (~50 μm), which may present similar negative impacts on alkalinity production. Sample FA, fly ash, is predominantly glassy (up to 50 % amorphous content), with the aluminium-silicate glass identified by SEM-EDS. The crystalline phases present show no realistic promise for alkalinity generation or carbonation. However, any amorphous phases (submicron phases, typically blanketing larger minerals, with Mg and/or Ca identified in the structure by EDS; examples shown in Fig. 3 g–i) may harbour some potential. Similarly, sample ACS is a glassy slag (up to 50 % amorphous content) of limited carbonation promise, though enstatite was identified as a crystalline phase by SEM-EDS.

3.4. Sample chemistry

Samples show geochemical compositions that reflect their mineralogy (Table 3). Dunite and Ni sulphide tailings samples show the highest MgO content (30–37 wt%, mostly reflecting high serpentine content), with fine-grained kimberlite tailings also exhibiting high MgO (~24 wt%, high olivine content). Ilmenite tailings and fine marble

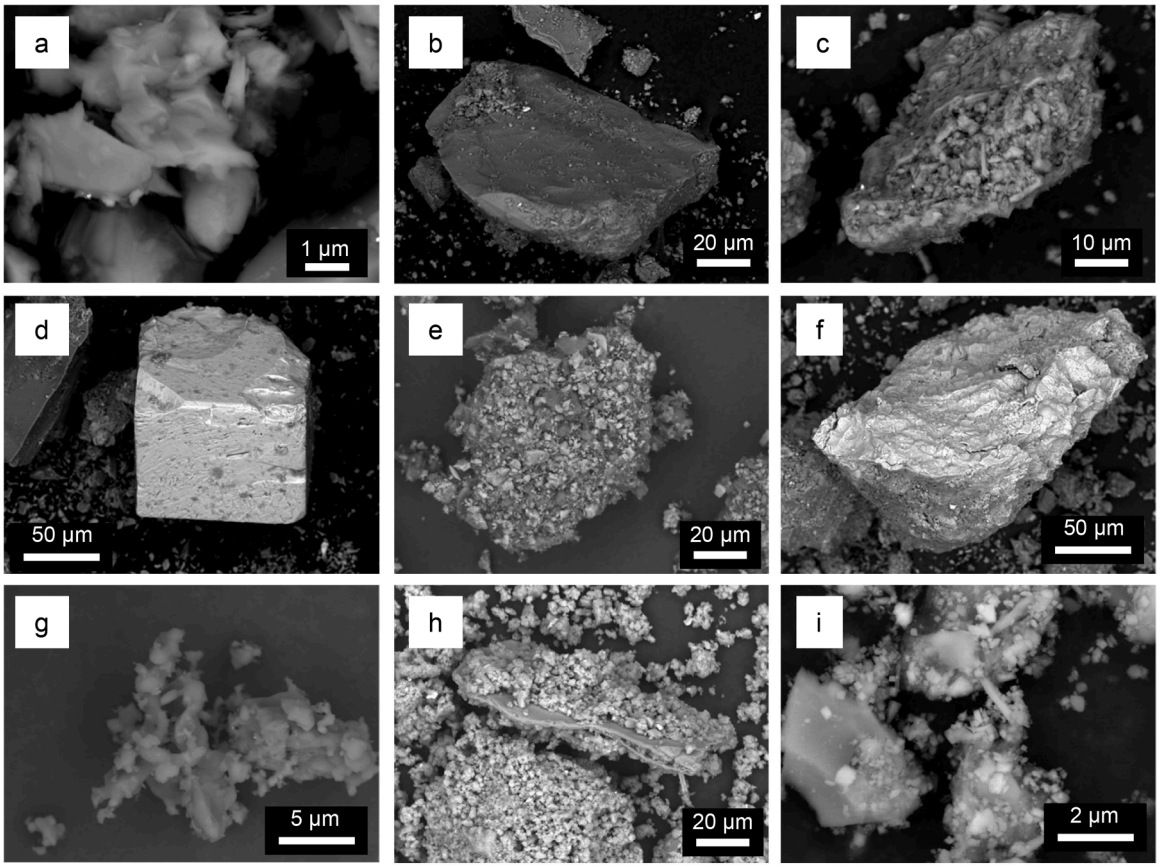

Fig. 3. SEM images of example mineralogy from select samples, including (a-c) minerals of interest for alkalinity generation, and (d-f) minerals that may hinder alkalinity production or promote acidity. (a) Rare brucite (Mg-hydroxide) is present in kimberlite tailings samples (image from sample ACT), (b) olivine (forsterite), typical in dunite and kimberlite samples (image from sample DK), (c) serpentine (lizardite), present in dunite and Ni sulphide tailings samples (image from sample DUL), (d) pyrite, present in Cu tailings and fluorite tailings samples (image from sample A-EP), and (e) thenardite (anhydrous Na sulphate) (image from sample BAP1), and (f) rhomboclase (Fe sulphate), both typical in borax tailings samples (image from sample A-ESC). Also shown are possible sub-micron amorphous phases in samples (g) BRP, (h) SCDS, and (i) RTKC.

cuttings show high CaO concentrations (48–51 wt%, reflecting high Ca sulphite, carbonate, and silicate content in ilmenite tailings, high carbonate (calcite) in marble fines; ~13 wt% TIC content in marble fines), while borax tailings and Al-red mud sample NRMS show high (>10 wt %) Na_2O contents (Na sulphates and borates). The ilmenite tailings sample also contains notably high S content (11 wt%) and TIC content (5 wt%). Tailings associated with Cu mining, as well as coarse kimberlite tailings, show high SiO_2 contents (65–87 wt%), reflecting high quartz content. The fly ash sample contains high TC content (26.7 wt%, all as TOC). Several samples show elevated trace element contents that may be a potential threat if liberated into local environments such as water and soil systems, particularly in Cu tailings and SO_2 processing plant by-products (SM Table II). These include notably high Ba content (>250 µg/g in diamond kimberlites, Cu tailings, fluorite tailings, and fly ashes), As (>130 µg/g in borax, Cu, and fluorite tailings), Co (>190 µg/g in SO_2 processing plant by-products and Cu slag glasses), Cu (>230 µg/g in Cu tailings and slags, Ni sulphide tailings, and SO_2 processing plant by-products), Ni (>500 µg/g in Ni sulphide and kimberlite tailings, and SO_2 processing plant by-products), Pb (>240 µg/g in Cu tailings and slags, and SO_2 processing plant by-products) and Zn (>200 µg/g in Cu tailings and slags, fluorite tailings, and SO_2 processing plant by-products).

4. Experimental results

4.1. Solution chemistry

At the experimental onset, the pH decline from neutral to more acidic conditions was driven by equilibration with CO_2 and the formation of DIC, prior to sample addition. Before sample additions, the starting solution showed a pH range of ~3.6 to 4.1, generally maintained throughout the 100-hr experiments by the blank samples (pH fluctuations ~±0.2). Over the sample set, final pH values range from 3.9 (Cu tailings sample A-ESC) to 7.0 (borax tailings sample BAP2), with Cu-related samples and the fly ash sample generally showing the lowest achieved pH values. In all sample cases, with the exceptions of Cu tailings samples RTKC, SDS, and A-ESC (and blank samples), alkalinity indicator measurements suggest the presence of carbonate (CO_3^{2-}) and bicarbonate (HCO_3^-) ions in solutions, with two borax samples (BAP2 and BRP) showing the highest alkalinity generation. For Cu tailings, alkalinity indicator measurements also suggest the presence of CO_2 and hydroxide (OH^-) in the solution.

After the addition of the solid samples, pH values generally showed a rapid increase in the first 2–4 hrs of the experiment, followed by levelling out, though some samples exhibited a slight gradual rise beyond that and for the remainder of the experiment (e.g., Ni sulphide, fly ash, and some Cu samples) (Fig. 4a). Conductivity, which may be used to indicate increased dissolved salts and other inorganic chemicals, shows similar trends to pH, with an initial rapid increase, followed by a more gradual increase or plateauing for the remainder of the experiment

Table 3
Starting compositions (major oxide (normalised), sulphur (S), total carbon (TC), and total inorganic carbon (TIC) weight percentages) of pre-experimental samples. Trace element concentrations shown in SM Table II.

Sample type	Units	Diamond kimberlite mine tailings			Dunite mine tailings		Al-red mud mine tailings		Borax mine tailings			Cu mine tailings				Cu slag material	Ilmenite mine tailings	SO_2 processing plant by-products	**Marble fine cuttings**	**Fluorite mine tailings**	**Ni sulphide mine tailings**	**Power plant fly ash**
Sample code		DFT	DK	ACT	DUL	DUN	GRM	NRMS	BAP1	BAP2	BRP	RTKC	SDS	A-ESC	A-EP	ACS	SCDS	SSO2	MAR	MFA	WCN	FA
SiO_2	wt%	45.4	46.6	76.8	40.9	40.3	15.3	17.7	8.3	1.9	4.1	61.1	87.1	71.6	65.8	28.5	2.0	12.2	0.7	67.5	35.5	44.8
TiO_2	wt%	0.5	0.5	0.9	0.2	0.2	6.5	7.2	–	–	–	0.3	0.2	0.2	0.1	0.3	28.7	37.6	–	0.1	0.1	0.8
Al_2O_3	wt%	6.0	6.5	6.3	3.4	2.5	24.9	20.4	1.7	0.4	0.6	6.0	3.7	5.8	8.4	3.7	0.6	6.0	0.1	1.4	2.6	20.7
Fe_2O_3	wt%	6.6	6.5	3.8	7.5	8.3	35.4	26.5	1.0	0.3	0.2	13.5	2.4	14.7	15.1	62.0	2.4	34.8	0.1	1.8	18.3	5.5
MnO	wt%	0.1	0.1	0.1	0.3	0.1	-	-	-	-	-	0.1	-	-	0.2	0.1	-	0.3	-	-	0.2	0.1
MgO	wt%	24.4	24.5	5.0	30.8	36.6	0.5	2.5	0.5	0.3	0.2	0.7	1.5	1.0	3.5	1.5	0.8	5.2	2.8	1.0	32.0	1.5
CaO	wt%	3.9	3.8	1.7	2.5	2.0	1.4	2.3	0.7	2.3	0.4	6.4	0.8	0.1	0.4	2.3	48.8	1.9	51.7	18.6	1.4	1.5
Na_2O	wt%	0.4	0.8	-	0.1	0.2	6.5	13.4	61.7	11.8	28.2	0.3	0.3	-	-	0.3	0.1	1.0	-	-	0.1	0.5
K_2O	wt%	1.6	1.9	1.9	0.1	0.1	0.2	0.2	0.7	0.1	0.2	3.4	2.2	0.7	0.6	1.1	0.1	0.5	-	0.5	0.1	3.2
P_2O_5	wt%	0.3	0.3	0.4	0.1	-	0.1	0.2	-	-	-	0.2	0.1	-	-	0.1	-	0.1	-	-	-	0.3
B_2O_3	wt%	-	-	-	-	-	-	-	12.5	59.7	24.5	-	-	-	-	-	-	-	-	-	-	-
LOI	wt%	10.6	8.4	3.0	14.1	9.7	9.2	9.6	13.0	23.2	41.7	8.0	1.6	5.9	5.9	-	16.5	0.4	44.6	9.1	9.7	21.0
Total	wt%	100	100	100	100	100	100	100	100	100	100	100	100	100	100	100	100	100	100	100	100	100
TC	wt%	1.4	1.2	0.1	2.2	0.1	0.4	0.8	0.1	0.06	0.1	0.05	0.03	0.04	0.5	0.01	5.4	0.4	13.2	1.5	0.1	26.7
TIC	wt%	0.6	0.6	0.04	0.4	0.1	0.2	0.6	0.1	0.03	0.04	-	0.02	-	0.4	-	5.3	0.1	12.9	1.5	0.1	-
S	wt%	0.5	0.4	-	-	-	0.1	0.4	13.5	4.4	-	3.3	1.2	0.9	2.0	0.6	11.2	0.3	0.1	1.2	4.0	0.8

(-) indicates a value below the level of detection.

(Fig. 4b). Conductivity may also positively correlate with total alkalinity, as demonstrated in natural water, soil, and land use trials (Amann and Hartmann, 2022; Bouillon et al., 2014; Proulx et al., 2018; Sechriest, 1960).

The greatest initial pH increase was associated with borax tailings samples BRP and BAP2, with BRP rising from 3.8 to 6.3 within an hour of the sample addition, and BAP2 rising from 4.7 after the sample was added (<1 h) to 6.7 after 2 h. This was mimicked in the BRP and BAP2 alkalinity indicator measurements, with rapid increases in Na_2O (up to 2990 mg/L after 2 h, 3170 mg/L after 7 h) and $NaCO_3$ (5382 mg/L after 2 hrs, 5706 mg/L after 7 h). Ilmenite mine tailings and Al-red mud mine tailings samples also exhibited a notably high initial rise (up to 6.0 after 2 h in the case of ilmenite tailings), as well as high final pH values (up to 6.2 for both sample types after 100 hrs). Fine-grained kimberlite and dunite tailings were closely grouped and follow similar trends throughout the experiment, with final pH values of 5.8 to 6.0. Cu tailings samples generally lacked the initial pH increase. In one case (sample A-ESC), pH values did not rise above the levels of the blank samples, suggesting the material was generally benign with CO_2-water reactions, with no apparent effect on pH or alkalinity generation (confirmed by no recorded changes in CaO or CaO_3 alkalinity indicators throughout the experiment) (Fig. 4c, d).

Elemental Ca, Mg, and Si release into the host solution was measured throughout the experimental duration (Fig. 5 and SM Table III). While Ca and Mg were measured for their role in alkalinity generation, Si concentrations of the solution were monitored due to the element acting as a key structural framework for silicate minerals (Oelkers, 2001; Marieni et al., 2020), thus acting as a control on mineral W_r in the majority of samples (with the exception of non-silicate-rich samples). Overall, the fastest Si, Ca, and Mg elemental release occurred in the initial 1–3 h of the experiment, when solution pH was at its lowest (pH ~3–4), before showing a more gradual rate of release or levelling out for the remainder of the experiment, coinciding with gradually rising or plateauing pH. Red mud and dunite samples showed the highest total Si release across the experiment, totalling ~34–60 mmol/L, with low Si release from fluorite tailings and the marble cuttings sample. Ilmenite tailings and marble cuttings showed the highest Ca release (total release of 648 and 550 mmol/L, respectively), while dunite tailings (136–173 mmol/L) and fine-grained kimberlite tailings (111–133 mmol/L) showed the highest Mg release. Select Cu tailings samples also showed notably high Mg (sample A-ESC, 44 mmol/L) and Ca (sample RTKC, 433 mmol/L) release.

4.2. Dissolution rates (W_r)

W_r values were derived based on Si, Ca, and Mg release across the entire experimental duration, using average starting BET-SSA-normalised values (Fig. 6, Table 4, and SM Table IV; G-SSA-normalised values also shown in SM Table IV). In general, G-SSA-normalised values were ~1 magnitude faster than BET-normalised values for this study, consistent with other studies (e.g., (Brantley and Mellott, 2000; Delerce et al., 2023; Renforth et al., 2015)). For Si release, BET-normalised values ranged across all samples ~−12 to −16 log (mol/cm^2/s), averaging ~−14 log (mol/cm^2/s) (Fig. 6a). For Ca and Mg release, values ranged ~−11 to −16 log (mol/cm^2/s) (Fig. 6b) and ~−12 to −16 log (mol/cm^2/s) (Fig. 6c), respectively. The fastest rates were associated with the initial hours of the experiment when the solution pH was at its lowest and finer fractions were present to provide an initial rapid rate of dissolution. W_r values gradually declined following the initial stages, coinciding with rising pH and removal of finer fractions into solution. Overall, samples with the fastest W_r (based on Si release) were typically borax tailings (average ~−13 to −14 log (mol/cm^2/s)), followed by dunite tailings, fly ashes, ilmenite tailings, and red mud samples.

Conversely, marble cuttings showed the fastest rates based on Ca release, averaging ~−11 to −12 log (mol/cm^2/s), with carbonate-rich

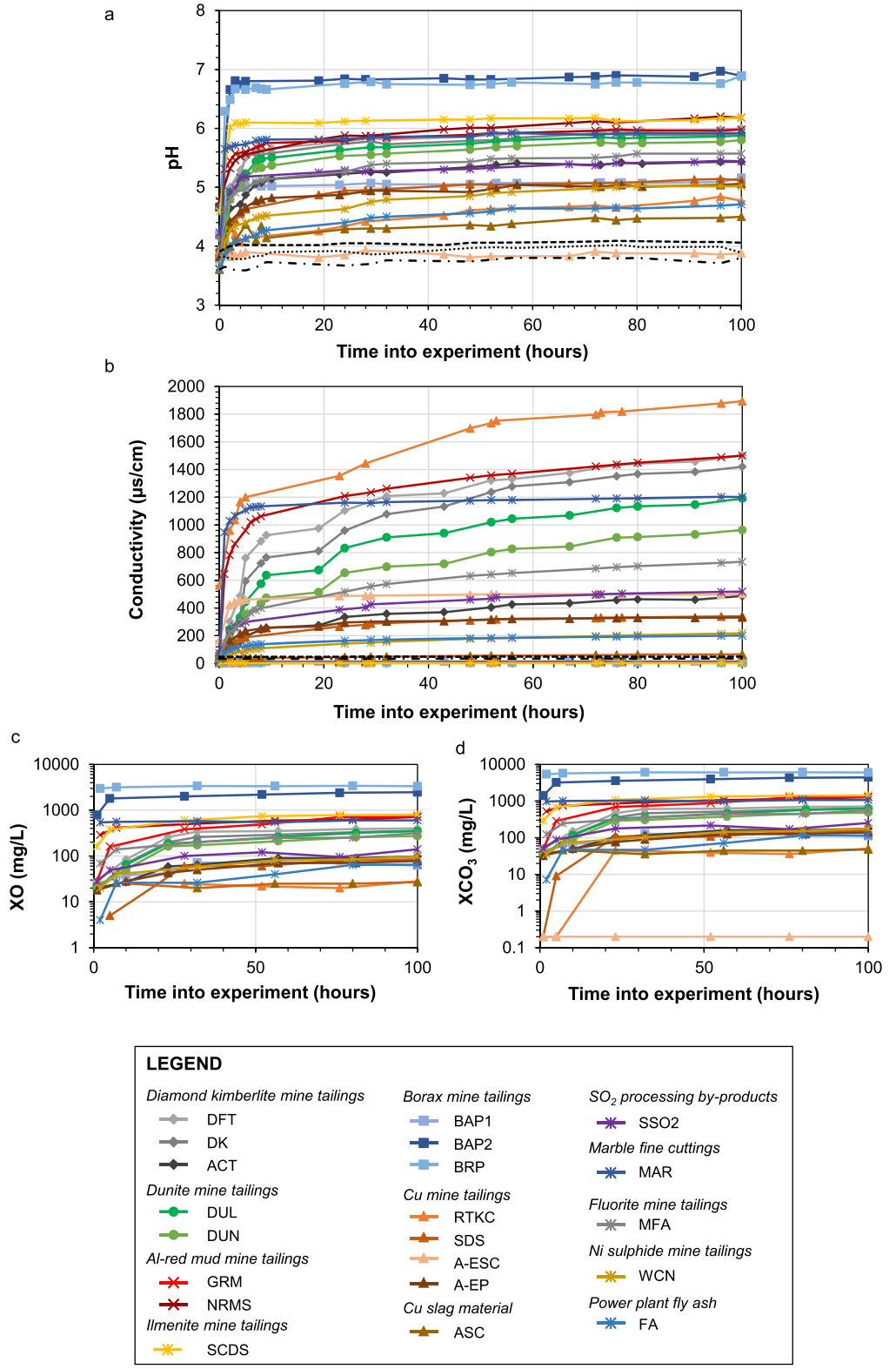

Fig. 4. Solution chemistry trends during the experiment. (a) pH change, (b) conductivity change, and (c, d) alkalinity indicators based on carbonate hardness, expressed as: (c) Oxide (e.g., CaO, MgO, Na_2O, major element depicted by X, and (d) XCO_3 in solution. Blank samples indicated by black dashed lines in (a, b).

fluorite tailings, ilmenite tailings, and borax tailings samples showing similar rates. For Mg release, the fastest W_r (~−13 to −14 log (mol/cm^2/s)) were dunite, Ni sulphide, borax, and fine kimberlite tailings, as well as marble cuttings, borax tailings (samples BAP1 and BRP), and one Cu tailings sample (A-ESC).

4.3. Changes in physical, chemical, and mineralogical sample properties

Solid samples were analysed post-experiment for their weight change, XRD modal mineralogy, BET-SSA change, and TC/TIC/TOC content changes. All borax mine tailings samples showed the highest loss

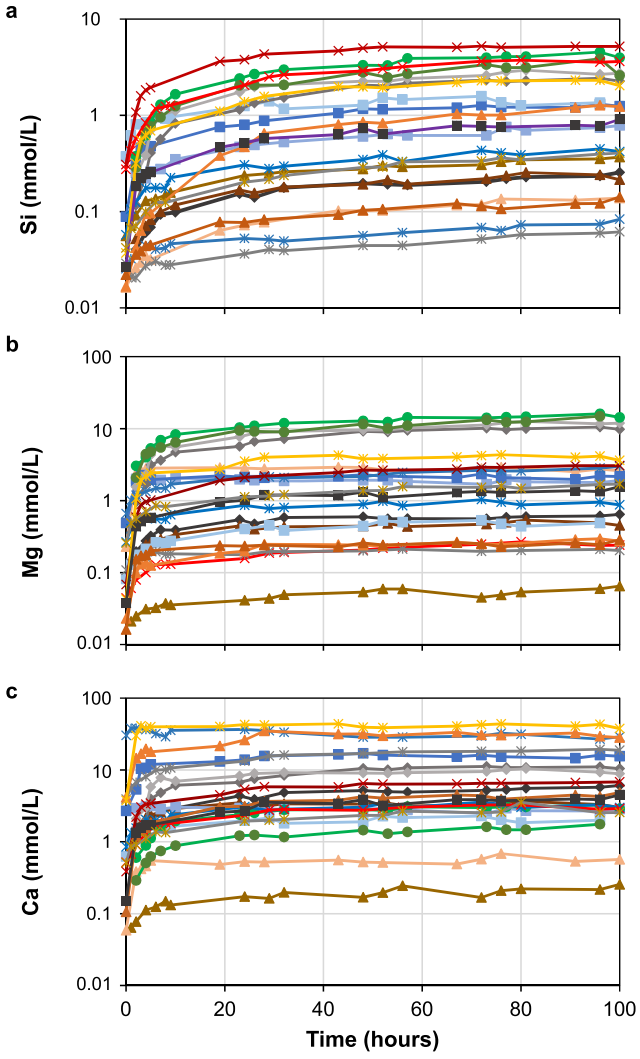

Fig. 5. Changes in cation concentrations in host media throughout the experimental procedure. (a) Si, (b) Mg, and (c) Ca. Symbols and colours as shown in Fig. 4.

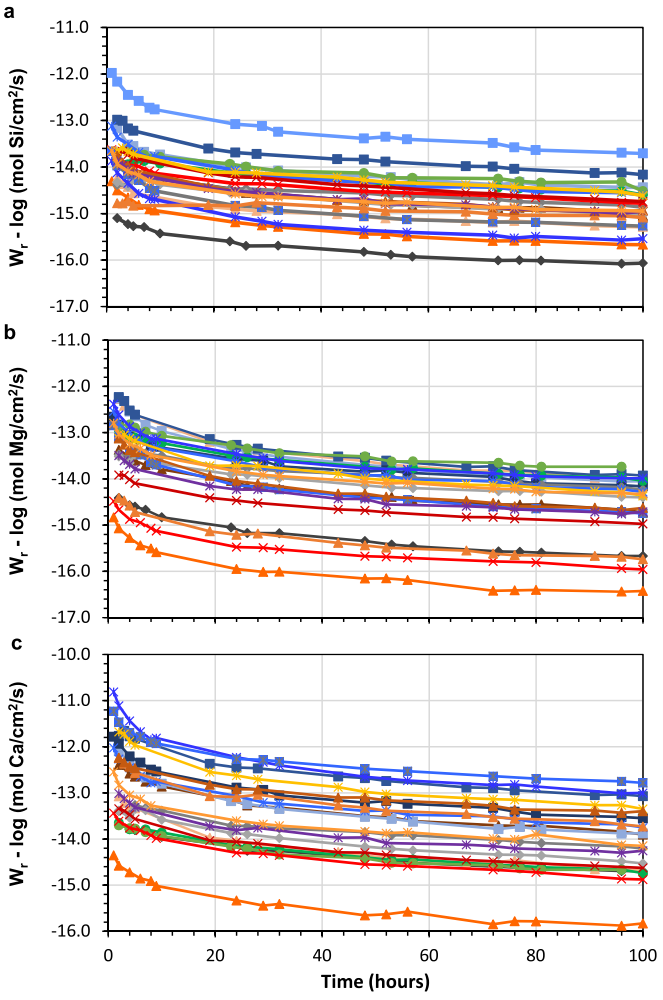

Fig. 6. Dissolution rates (W_r) of industrial by-product samples analysed in this study, normalised to the BET-SSA, based on (a) Si release, (b) Mg release, and (c) Ca release. Symbols and colours as shown in Fig. 4.

of solid sample from pre- to post-experiment (~1–5 % of original sample weight remaining post-experiment), while kimberlite fines (~26–32 % sample loss), the sample from SO_2 processing (~30 % sample loss), select Cu tailings samples (RTKC ~25 % sample loss), Al red mud samples (~13–19 % sample loss), dunite tailings (~12–17 % sample loss), and the marble quarry fines (~12 %) also exhibited a notable sample decrease post-experiment (SM Table V). The Cu slag, fluorite tailings, Ni tailings, and fly ash samples all showed >90 % sample retention post-experiment. Excluding kimberlite sample ACT, fluorite tailings, and borax mine tailings samples, all samples showed a post-experimental increase in BET-SSA (Fig. 7a). Cu tailings sample A-ESC showed the greatest increase from 3 m^2/g to 23 m^2/g, while samples DFT, DUL, and GRM also exhibited notable increases (SM Table VI). Samples ACT and MFA decreased in post-experimental BET-SSA, while there was insufficient material remaining for post-experimental analysis of borax tailings samples.

The most notable modal mineralogical change from pre-experimental to post-experimental, as determined by XRD (Table 5), was the significant reduction in borax, thenardite, sassolite, halite, tincalconite, and ulexite in borax tailings samples (BAP1, BAP2), with high calcite content (67 % modal mineralogy, where previously not identified pre-experiment) noted in sample BAP2. There was also a notable reduction in portlandite in the ilmenite mine tailings (from 22.6 % pre-experiment to none identified post-experiment), while calcite content rose from 16 % modal abundance to 53 % modal abundance in the same sample. Basanite ($CaSO_4{\cdot}0{\cdot}5H_2O$) was also present post-experiment in ilmenite tailings, with reductions in hannebachite abundances evident. Calcite showed modal reductions in select kimberlite (DK, DFT) and red mud samples (as well as sodalite abundance reduction in sample NRMS), while nontronite was evident in select kimberlite (DFT) and Cu mine tailings (SDS) samples post-experiment. Sample DFT also showed the post-experimental presence of muscovite and lizardite, and red mud sample GRM showed post-experimental boehmite present. It should be stressed that

XRD can only characterise crystalline solid phases, meaning any possible amorphous phases (which may contain Ca or Mg) present in the samples would be not identified using this technique. The presence of amorphous phases is therefore inferred here in the majority of samples, based on the large diffuse bump XRD pattern (with high-intensity narrow peaks superimposed to indicate more structured crystalline phases) and sporadic evidence for amorphous-like powdered morphologies identified by SEM (containing variable amounts of Ca and Mg, based on EDS; Fig. 3 g–i). Of the twenty one samples, fourteen showed a reduction in amorphous content (including notably large reductions in samples DFT and DUN), four samples showed a content increase and three showed no recorded change. Post-experimental amorphous content also generally correlates positively with post-experimental BET-SSA.

Table 4
Summary of dissolution rates (W_r), calculated over the 100-hour experimental duration, normalised to the BET-SSA, based on Si, Mg, and Ca release. Full Wr dataset, including BET and geometric (SSA)-normalised rates, shown in SM Table IV.

	Si-derived W_r			Mg-derived W_r			Ca-derived W_r		
	log (mol/cm²/s)			*log (mol/cm²/s)*			*log (mol/cm²/s)*		
Sample	Average	Minimum	Maximum	Average	Minimum	Maximum	Average	Minimum	Maximum
Diamond kimberlite mine tailings									
DFT	−14.54	−14.87	−14.25	−13.83	−14.23	−13.37	−13.77	−13.26	−13.26
DK	−14.66	−15.04	−14.26	−13.98	−14.4	−13.48	−13.98	−14.53	−13.35
ACT	−15.7	−16.08	−15.1	−15.17	−15.67	−14.41	−14.27	−14.69	−13.67
Dunite mine tailings									
DUL	−14.22	−14.6	−13.85	−13.58	−14.04	−12.95	−14.24	−14.74	−13.65
DUN	−14.02	−14.33	−13.65	−13.35	−13.74	−12.82	−14.25	−14.67	−13.7
Al-red mud mine tailings									
GRM	−14.32	−14.78	−13.63	−15.39	−15.96	−14.48	−14.27	−14.88	−13.44
NRMS	−14.25	−14.74	−13.66	−14.52	−14.97	−13.92	−14.1	−14.63	−13.34
Borax mine tailings									
BAP1	−14.02	−14.44	−13.16	−13.42	−14.06	−12.26	−13.25	−13.88	−12.09
BAP2	−13.71	−14.17	−12.98	−13.32	−13.93	−12.23	−12.51	−13.07	−11.66
BRP	−13.08	−13.71	−11.98	−13.59	−14.16	−12.66	−12.89	−13.55	−11.78
Cu mine tailings									
RTKC	−14.9	−15.09	−14.74	−15.25	−15.74	−14.41	−13.15	−13.73	−12.24
SDS	−14.55	−14.98	−13.76	−14.11	−14.67	−13.13	−12.97	−13.43	−12.24
A-ESC	−14.9	−15.29	−14.24	−13.34	−14.01	−12.27	−14.06	−14.68	−13.07
A-EP	−14.57	−15.05	−13.89	−14.17	−14.73	−13.38	−13.28	−13.9	−12.39
Cu slag material									
ACS	−15.2	−15.67	−14.31	−15.9	−16.44	−14.84	−15.33	−15.88	−14.35
Ilmenite mine tailings									
SCDS	−14.17	−14.62	−13.59	−13.81	−14.37	−13.05	−12.71	−13.35	−11.68
SO_2 processing plant by-products									
SSO2	−14.58	−14.99	−13.87	−14.29	−14.76	−13.5	−13.83	−14.3	−13.01
Marble fine cuttings									
MAR	−15.01	−15.57	−13.87	−13.44	−13.99	−12.38	−12.22	−13.01	−10.81
Fluorite mine tailings									
MFA	−14.72	−15.27	−13.66	−14.02	−14.75	−12.85	−12.18	−12.78	−11.23
Ni sulphide mine tailings									
WCN	−14.55	−14.95	−13.65	−13.83	−14.33	−12.8	−13.6	−14.15	−12.54
Coal-fired power plant fly ash									
FA	−14.08	−14.6	−13.12	−13.65	−14.28	−12.54	−13.11	−13.75	−12.02

With the exceptions of samples which contained no pre-experimental TIC content (samples RTKC, A-ESC, ASC, and FA), samples which had no remaining material post-experiment (borax tailings sample), dunite (DUN), ilmenite, and Ni sulphide tailings samples, all other samples showed an increase in TIC% from pre-experiment to post-experiment (Fig. 7b and SM Table VII). Samples ACT, GRM, SSO2, and SDS showed the greatest post-experimental percentage increase (~150–725 % increase), while samples NRMS, A-EP, and MAR showed minor increases (up to 12 % increase). Dunite tailings sample DUN showed the same TIC content pre- and post-experiment (0.1 %). Ilmenite tailings sample SCDS showed a decrease in TIC (5.34 % content to 2.6 % content), while Ni sulphide tailings sample WCN showed a percentage decrease of 44 % (0.09 % content to 0.05 % content). By comparison, the majority of samples show reductions in TOC content (SM Table VII).

4.4. Geochemical modelling of precipitates

The predictive results of the PHREEQC secondary precipitate calculations are shown in Table 5 and SM Table VIII. The calculated outputs of interest for this study were any predicted carbonate phases, indicating that possible geochemical CDR by means of mineral carbonation could theoretically be achieved, particularly in samples that did not contain carbonates in the original material. Across the sample suite, several carbonates were identified as possible precipitates: artinite ($Mg_2(CO_3)(OH)_2{:}3H_2O$), dolomite ($CaMg(CO_3)_2$), magnesite ($MgCO_3$), huntite ($CaMg_3(CO_3)_4$), hydromagnesite ($Mg_5(CO_3)_4(OH)_2{:}4H_2O$), and nesquehonite ($MgCO_3{:}3H_2O$). Samples with predicted precipitated carbonates were kimberlite tailings (artinite, huntite, hydromagnesite, magnesite, and nesquehonite identified), dunite (huntite, magnesite, and nesquehonite), ilmenite tailings (dolomite), and Ni sulphide tailings (dolomite and magnesite). Most samples were predicted not to generate carbonates, instead producing various Al-K-Na-Mg-Ca-Fe secondary precipitates, predominantly aluminosilicate clays (e.g., nontronite (recognised by XRD in some post-experimental samples), halloysite, kaolinite), Al-Si hydroxides (e.g., boehmite, diaspore, pyrophyllite), Fe-oxides (e.g., haematite, lepidocrocite), hydrous sulphates (e.g., jarosite, aluminite), and SiO_2 polymorphs (e.g., quartz, cristobalite, chalcedony). Many of these non-carbonates (including some containing Ca and Mg) were predicted to precipitate in samples where carbonates were also supersaturated (minerals competing for available cations).

5. Discussion

5.1. Cation sources and dissolution rates

In the kimberlite tailings samples, calcite and dolomite are considered cation sources for the high Ca in solutions, with forsterite, dolomite, clinochlore, chrysotile, and talc potentially providing additional sources for Mg release, as well as minor brucite phases. The higher concentrations of Ca compared to Mg in solution in these samples, despite higher MgO contents compared to CaO of the starting solid materials, suggests faster Ca release from calcite compared to Mg release from dolomite and other Mg-bearing silicate sources. Dolomite, along with tremolite, likely provided the Ca sources in the dunite tailings samples, with Mg sourced from dolomite, and contributions from slower-reacting forsterite, lizardite, tremolite, enstatite, and clinochlore. Calcite was responsible for high Ca release in the Al red mud samples. In contrast, the Ca and Mg release identified in borax tailings samples may have been sourced from ulexite and clinochlore respectively. In these samples, high alkalinity generation is attributed to Na-rich minerals and

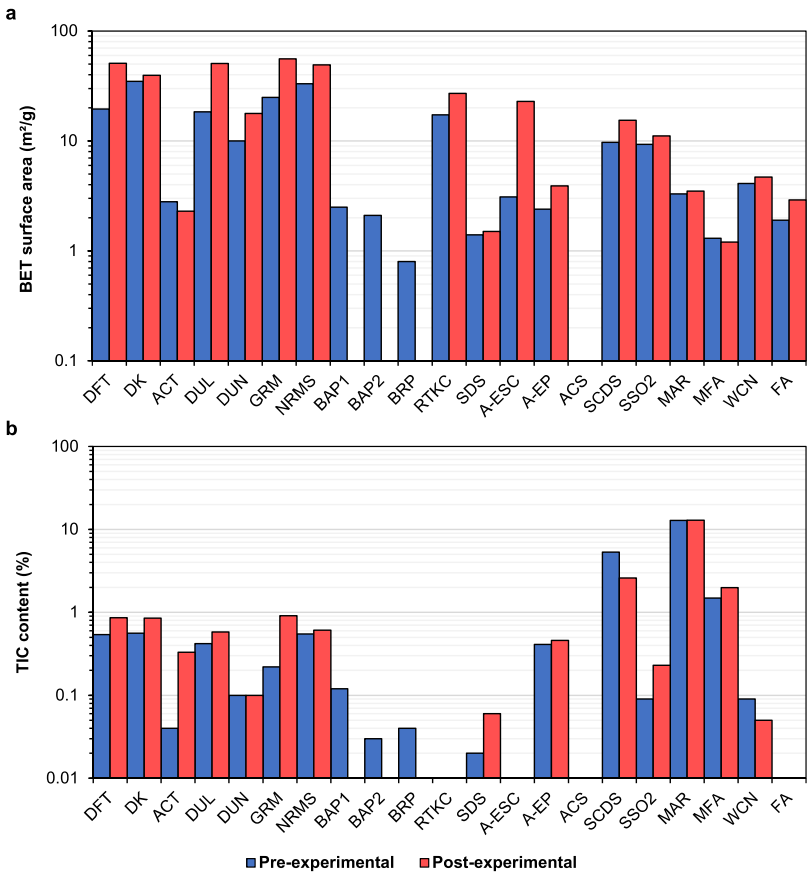

Fig. 7. Changes to physical and chemical sample properties from pre- to post-experiment: (a) Pre- and post-experimental BET-SSA (m^2/g), there was insufficient material remaining for post-experimental analysis of borax tailings samples. (b) Pre- and post-experimental total inorganic carbon (TIC) sample contents (%); samples RTKC, A-ESC, ASC, and FA contained no pre-experimental TIC content and borax tailings samples had no remaining material post-experiment.

boron phases (borax and tincalconite). In Cu tailings, high Ca release associated with sample RTKC may be a product of gypsum dissolution (with some possible minor Ca and Mg contributions from Ca-Mg-bearing clays), while high Mg release in sample A-ESC may have been sourced from clinochlore and amorphous phases. The ilmenite tailings host several potential Ca sources (fast-reacting portlandite, as well as hannebachite, calcite, and thaumasite), and Mg may have been sourced from magnesite and phlogopite. SO_2 processing plant by-products with high Ca release may have been sourced from anorthite (with Mg possibly sourced from clinochlore), while in the marble cuttings sample, Ca and Mg were sourced from calcite and dolomite, respectively. Fluorite, calcite, and dolomite (with possible contributions from illite) were responsible for Ca and Mg release in the fluorite tailings sample, while tremolite (Ca) and lizardite, clinochlore, and tremolite (Mg) likely provided the cation sources for the Ni sulphide tailings sample.

The two glassy samples (Cu slag and power plant fly ash), which contain limited crystalline phases of limited reactivity and cation content, likely sourced their Ca and Mg release from cation-hosting amorphous phases (constituting up to 50 % of the sample material). Glassy slag and fly ash samples contain abundant amorphous materials, resulting from heating and rapid quenching processes. Amorphous materials in samples are suggested to supply cations that were released into solution during experimentation, where apparent crystalline sources are generally lacking (e.g., glassy slag and fly ash samples, and possibly some red mud, Cu, and borax tailings samples). The presence of cation-bearing amorphous material could also explain high cation release in samples that contain minerals that generally undergo slow dissolution (i.e., most silicate phases), as glassy phases may react similarly to, or even more rapidly than, phases such as olivine (Gislason and Oelkers, 2003; Kelemen et al., 2011, 2020).

As anticipated based on mineralogy, the highest cation release for Ca and Mg was associated with dunites, kimberlites, and marble cuttings, making these the preferred cation sources. These samples host multiple Ca-Mg source minerals, with carbonate minerals (calcite, dolomite) most likely to produce alkalinity due to their comparatively fast W_r compared to Mg-Ca silicates. Such silicates may have also contributed Ca-Mg cations in the dunite and kimberlite samples, particularly saponite (identified by SEM-EDS in kimberlite samples), lizardite, chrysotile, and forsterite, as well as any rare hydroxide phases present, such as brucite (identified by SEM-EDS in kimberlite samples) and any Ca-Mg-bearing amorphous material present. Dunites, Ni sulphides, and kimberlites are known for their CDR potential due to their high Ca-Mg cation content in silicate and hydroxide minerals (Bullock et al., 2021; Kremer et al., 2019; Schuiling and Krijgsman, 2006; Wilson et al., 2009a, 2014; Lacinska et al., 2017; Mervine et al., 2018; Rigopoulos et al., 2015; ten Berge et al., 2012), while carbonate-rich deposits have also been targeted for *ex-situ* CDR processes (Caserini et al., 2021; Foteinis et al., 2022; Rau, 2008; Rau and Caldeira, 1999; Renforth and Henderson, 2017; Renforth et al., 2013). Ilmenite tailings also show notably high Mg and Ca release, owing to the high portlandite (fast reacting Ca-hydroxide) and calcite content to produce alkalinity, while select Cu tailings samples also show higher release than the majority of samples (in particular, samples containing crocidolite). Conversely, high silica, low Ca-Mg Cu slags and Cu tailings are undesirable for CDR purposes. Furthermore, solution pH of Cu slag and tailings samples after 100 h was in the range 3.9–5.1. In practical applications, host conditions (e.g., water-saturated soils) with a pH <5.2 may be considered unsuitable candidates for CDR approaches, as dissolution of minerals by

Table 5
Post-experimental modal mineralogical changes (determined by XRD) and predicted carbonate precipitation phases from CO_2-water-material reactions of samples, assuming continued reaction time to full conversion of any Ca- and Mg-bearing minerals present, under experimental conditions, produced by PHREEQC modelling using the MINTEQ database.

Sample	Post-experimental mineralogical changes (determined by pre- and post-experimental XRD)	Post-experimental amorphous content (%)	Predicted carbonate precipitation phases (determined by PHREEQC)
Diamond kimberlite mine tailings			
DFT	Lizardite present in post-experimental sample	45.5	Artinite; huntite; hydromagnesite; magnesite; nesquehonite
DK	-	37.0	Artinite; huntite; hydromagnesite; magnesite; nesquehonite
ACT	-	4.4	Dolomite; magnesite
Dunite mine tailings			
DUL	-	20.6	Huntite; magnesite; nesquehonite
DUN	-	18.4	Magnesite
Al-red mud mine tailings			
GRM	Boehmite (Al-(oxy) hydroxide) present in post-experimental sample	50.0	ND
NRMS	Halite is not present in post-experimental sample, but was identified pre-experiment	50.0	ND
Borax mine tailings			
BAP1	Clinochlore and pargasite (Na-Ca-Mg-amphibole) present post-experiment; halite, rhomboclase, and sassolite not present post-experiment	12.0	ND
BAP2	Calcite and pargasite present post-experiment; borax, thenardite, tincalconite, and ulexite not present post-experiment	9.9	ND
BRP	Insufficient amount of material remaining for XRD	-	ND
Cu mine tailings			
RTKC	-	10.9	ND
SDS	Nontronite (smectite group mineral) present post-experiment	2.7	ND
A-ESC	-	7.3	ND
A-EP	-	8.3	ND
Cu slag materials			
ACS	-	50.0	ND
Ilmenite mine tailings			
SCDS	Bassanite (Ca-sulphate) present post-experiment, large increase in calcite post-experiment; portlandite not present post-experiment	15.5	Dolomite
SO_2 processing plant by-products			
SSO2	-	35.0	ND
Marble fine cuttings			
MAR	-	5.3	ND
Fluorite mine tailings			
MFA	-	3.3	ND
Ni sulphide mine tailings			
WCN	-	11.5	Dolomite; magnesite
Power plant fly ash			
FA	-	48.1	ND

Hyphen (-) indicates no changes to minerals present (though changes to modal abundances may have occurred), ND indicates no carbonate phases identified in PHREEQC output.

non-carbonic acids would not produce alkalinity, thus reducing removal efficiency (Dietzen and Rosing, 2023).

Aluminium red muds show evidence of calcite dissolution through post-experimental reductions in modal contents. Though subject to more limited studies, red muds have been pinpointed for their CDR potential (Bonenfant et al., 2008; Renforth, 2019). While Al and Fe could increase alkalinity in very low or high pH solutions, in some conditions they may have the opposite effect on alkalinity contributions. The solubility of Al and Fe secondary oxides and clays is also very low, effectively removing these phases from the solution. Any secondary formation of Fe-carbonates would require strong reducing conditions to prevent the production of Fe-oxides and CO_2 (Renforth, 2019). Samples with high sulphide and sulphate mineral contents, prominent in Cu tailings-derived samples (e.g., pyrite identified in A-EP, baryte, and jarosite in A-ESC, gypsum in sample RTKC) and borax tailings samples (e.g., rhomboclase and thenardite), are likely to impact the carbonate system to produce CO_2 through acidity production. Similarly, materials treated with sulphuric compounds, such as those that may be present naturally in Ni sulphide tailings and enriched by industrial processes in mud products from SO_2 processing, may also rapidly produce Ca- and Mg-bearing sulphate minerals. The Ilmenite tailings sample contains high amounts of highly reactive portlandite, as well as thaumasite, calcite, and phlogopite, suitable for CDR purposes. However, high amounts of sulphate, sulphide or sulphite minerals such as hannebachite (present in this study) may pose a problem for CDR, as well as any potentially toxic trace elements with affinities to S that may also be present (e.g., As, Se) and create environmental risks. As borate can act to catalyse the conversion of CO_2 to HCO_3^- (Guo et al., 2011), the high abundance of Na-bearing borax and tincalconite in borax mine tailings samples may also be of particular interest for CO_2 reactivity.

Dissolution here is typically incongruent, indicated by the continual gradual increase in cation concentrations over 100 h of experimental time, the result of the non-stoichiometric release of the solid phase components, common in multicomponent minerals and mineral systems (Colman, 1981; Ruiz-Agudo et al., 2012, 2014), with concurrent precipitation of secondary minerals (e.g., clays) also affecting the net stoichiometry of the fluid composition. Regarding favourable W_r, borax tailings, dunite tailings, fly ashes, ilmenite tailings, and red mud samples show the highest Si-derived rates, while marble cuttings, fluorite tailings, and ilmenite tailings show the highest Ca-derived rates. The highest Mg release rates correspond to dunite, Ni sulphide, borax, and fine kimberlite tailings. These results suggest that dunite, kimberlite, red muds, and ilmenite tailings show the highest cation release concentrations and W_r.

In terms of desired W_r for meaningful CDR on human timescales, rates calculated here are comparable to those determined in previous studies for minerals and rocks that are typically targeted for geochemical CDR feedstock, such as olivine, basalt, and gabbro (typical W_r range of −12 to −14.5 log (mol/cm^2/s); (e.g., Crovisier et al., 1987; Eick et al., 1996; Gislason and Oelkers, 2003; Gudbrandsson et al., 2011; Gysi and Stefánsson, 2012; Marieni et al., 2020; Pokrovsky and Schott, 2000; Stockmann et al., 2012; Wolff-Boenisch et al., 2004). Of these examples, some include experiments conducted under CO_2-saturated conditions (e.g., Gysi and Stefánsson, 2012; Marieni et al., 2020; Pokrovsky and Schott, 2000), akin to the methods utilised in this study, and achieving similar rates, ~12.3 to −14.1 log (mol/cm^2/s), to the range of the majority of samples in this study.

Though care was taken to subject samples to equal conditions during experimentation, it is important to note critiques during data evaluation. The varied environmental and industrial settings (such as different processing and storage conditions) that the samples originate from will have varied effects on achieved W_r and possible secondary precipitates,

pre- and syn-experiment. Timescales, treatment, and degree of exposure to the atmosphere (or other conditions) at each sample origin site are unknown, which may have an effect on the amount of "natural" dissolution and/or precipitation that has already taken place. Samples of hyperalkaline state, such as red muds, also experience different effects with the addition of CO_2 during the experiment, potentially reducing pH and invoking carbonation or rapid production of Ca-bearing clays, silicates, and hydroxides. It should be noted that W_r achieved in the initial stages of the experiments may be elevated due to very fine particles formed during the powdering attaching to the solids. However, this may also be the case in industrial settings where materials are also typically crushed routinely as part of conventional management processes (e.g., commodity extraction, storage practices).

5.2. Carbonate precipitation

High post-experimental solid sample loss in borax samples indicates high-water solubility of sulphate and borate minerals present in samples, such as thenardite, borax, and tincalconite. More limited sample loss in kimberlite and dunite samples may indicate the dissolution of carbonates (also the case for the marble fines sample) and some dissolution of forsterite, serpentine group minerals, talc, and amorphous content. Sample loss in Al red muds, SO_2 processing muds, and select Cu tailings samples may indicate the dissolution of clay minerals under acidic conditions. Post-experimental XRD results suggest complete portlandite dissolution in ilmenite tailings and possible calcite dissolution in red muds (alongside sodalite) and select kimberlite tailings. High modal abundances of calcite in post-experimental ilmenite tailings suggest carbonate precipitation may have been achieved on short (1–3 weeks) timescales, likely owing to the high degree of Ca saturation in the solution. Significant borax, thenardite, tincalconite, sassolite, and ulexite dissolution is also inferred from post-experimental XRD results of select borax tailings samples, with notable calcite precipitation apparent in the post-experimental BAP2 sample. The BAP2 sample solution reached pH 7, possibly permitting carbonate precipitation in short (<100 hour) timescales under supersaturated carbonate conditions, with available nucleation sites (seed crystals) for secondary carbonates created from significant mineral dissolution of pre-existing phases.

PHREEQC modelling of CO_2-water-material reactions undertaken here suggests that some carbonates, such as artinite, dolomite, magnesite, huntite, hydromagnesite, and nesquehonite, may precipitate from solution in some of the sampled materials, should reactions be permitted to continue towards completion. Mg-carbonates such as magnesite and dolomite may precipitate slowly at low temperatures (Arvidson and Mackenzie, 1997; Lippmann, 1973; Pokrovsky and Schott, 2000; Banerjee, 2016, Gautier et al., 2014; Giammar et al., 2005; Power et al., 2019; Saldi et al., 2009, 2012). Magnesite is the most stable Mg-carbonate over a wide range of temperatures but is reluctant to form at ambient temperatures, typically requiring temperatures of 60–80 °C to form in aqueous solutions (Gautier et al., 2014; Hänchen et al., 2008; Saldi et al., 2009, 2012; Usdowski, 1989). As a consequence of the inhibitions to formation, numerous metastable hydrated Mg-carbonates are more typically formed at lower temperatures (Power et al., 2019), where the kinetic barriers for artenite, hydromagnesite, and nesquehonite growth are much lower (Hänchen et al., 2008; Hopkinson et al., 2012). This kinetic favourability reflects the Gay-Lussac-Ostwald or Ostwald step rule, whereby nucleation of more soluble phases, such as amorphous or metastable phases, is kinetically favoured over less soluble equivalents due to the lower interfacial energy between minerals and water (Langmuir, 1997). In sufficiently highly supersaturated solution, phases rapidly nucleate, precipitating low crystallinity and/or amorphous material (Langmuir, 1997; Sanjuán et al., 2019) (Fig. 3 g–i). Such hydrated Mg-carbonates have also been shown to co-exist under atmospheric conditions (Giampouras, 2020; Kloprogge et al., 2003).

Primary dolomite can precipitate directly from an aqueous solution, mostly under near ambient temperatures, with no $CaCO_3$ dissolution involved (Baker et al., 1994; Chakrabarti et al., 2011; Curtis et al., 1963; Land, 1973; Magenheim and Gieskes, 1992; Plumlee et al., 1994; Rosen et al., 1989; Tucker, 1982; Weber, 1964; Wells, 1962). Dolomite precipitation is favourable in aqueous solution with high Mg^{2+}/Ca^{2+} and carbonate alkalinity, elevated temperatures, and a high degree of supersaturation (Compton, 1988; Machel, 2004). Microbial activities can also promote dolomite formation at ambient temperatures (Liu et al., 2023; McKenzie and Vasconcelos, 2009; Roberts et al., 2004; Sánchez-Román et al., 2008; Van Lith et al., 2003 Vasconcelos and McKenzie, 1997; Vasconcelos et al., 1995). The presence of secondary nesquehonite and hydromagnesite has been identified in several carbonation studies, such as in basalt dissolution (Matter et al., 2016; Pogge von Strandmann et al., 2019), in brucite-rich mine tailings, whereby brucite was carbonated to form nesquehonite, and in other serpentine-rich deposits and tailings (e.g., Hostetler et al., 1966; Mumpton and Thompson, 1967; Wilson et al., 2009a; Lu et al., 2023; Oskierski, 2013; Wilson et al., 2011), where Mg for the formation of hydromagnesite and nesquehonite was predominantly derived from both brucite and Mg-silicate mineral sources.

The modelled results suggest that the ilmenite, Ni sulphide, kimberlite, and dunite tailings are highly suitable for any implemented schemes involving alkalinity production and carbonate precipitation, such as for any on-site solid output storage (e.g., carbonate storage in tailings dams). As well as carbonate precipitation, several aluminosilicate clays, Al-Si hydroxides, Fe-oxides, hydrous sulphates, and SiO_2 polymorphs were also predicted to form in these samples. Though these phases do not directly act to remove CO_2, their presence is still important for the overall CDR capacity, as they compete for available cations during precipitation. The solubility of Fe and Al secondary minerals is very low, so their precipitation strips most of the Al and Fe from the solution (Renforth, 2019). Sulphates that are present may have no implicit reaction with CO_2 (e.g., $CaSO_4 \rightarrow Ca^{2+} + SO_4^{2-}$) or may become acid compounds, impacting the carbonate system to produce CO_2 ($H_2SO_4 + 2HCO_3^- \rightarrow SO_4^{2-} + 2CO_2 + 2H_2O$) (Renforth, 2019). Fe and Al may also form complexes with OH^- in solution over a wide pH range, meaning their contributions to alkalinity may vary from positive to negative. At low pH, Al and Fe could contribute to CDR through increased alkalinity or the precipitation of iron carbonate ($FeCO_3$). However, the formation and stability of iron carbonate are influenced by redox conditions, and oxidation produces Fe-oxide and CO_2 (Renforth, 2019), although favourable conditions could be maintained in underground storage conditions.

While their contributions to alkalinity are still considered here, the practicalities whereby alkalinity is produced, CDR is effectively achieved, and precipitation is prevented or suppressed would require further considerations for marble fines. Direct and indirect CDR applications of carbonate rocks (such as marble cuttings) have been proposed for enhanced weathering and ocean alkalinity modification strategies (typically with limestone as a feedstock, e.g., Caserini et al., 2021; Harvey, 2008; House et al., 2007; Kirchner et al., 2020; Moras et al., 2022; Rau and Caldeira, 1999; Rau et al., 2007; Renforth et al., 2013). The aim with such carbonate-rich feedstocks is to utilise a sufficiently fast-reacting cation source for increased alkalinity (i.e., storage as bicarbonate in marine settings), before secondary carbonate precipitation occurs. These samples are therefore unsuitable for CDR methods targeting mineral carbonation. Although alkalinity production may be the preferred CDR route in terms of net CO_2 uptake (>1.5 mol of C removed for every mole of Mg or Ca dissolved from silicate minerals, 0.5 mol for carbonate minerals; Renforth and Henderson, 2017), carbonation and secondary precipitation of silicate-rich feedstocks may offer a more practical means of geochemical CDR for industry, as on-site management of solid products is likely to be easier to manage, monitor, and control compared to effluent outflows to groundwater, river, and ocean systems. Furthermore, precipitation of carbonates and other secondary minerals may provide an elemental sink to remove potentially toxic trace elements (e.g., Ba, As, Co, Cu, Ni, Pb, Zn, Se) from entering local

water systems or even concentrate potentially economic elements for future exploitation means. Co-application of CDR feedstocks such as biochar (Janssens et al., 2022), or the inclusion of certain types of fungi (Ruibal et al., 2005), in CDR strategies (e.g., enhanced weathering on amended croplands) can also potentially mitigate trace element release through retention, whilst also achieiving additional CDR. If applied in an agricultural setting, such synergistic combinations can also lead to improved soil health and increased crop productivity (Hagens et al., 2023; Rizwan et al., 2016; te Pas et al., 2023). Precipitation of typical secondary phases such as Fe-oxides and clays can also remove trace elements from solution through adsorption onto mineral surfaces, development of thin coatings or separate particles, substitution for other elements in the precipitated mineral phase, or physical capture (Bullock et al., 2019; Kısakürek et al., 2004; Stipp et al., 2002). Secondary precipitation of silica-rich layers at the surface of primary minerals, particularly evident in some silicate minerals, can hinder mineral dissolution and carbonate precipitation (Béarat et al., 2006; Harrison et al., 2015;Kremer et al., 2022; Ruiz-Agudo et al., 2012), requiring additional consideration to improve carbonation reactivity (e.g., the use of additives to enhance silica dissolution;, (Demadis and Mavredaki, 2005); sonication approaches to enhance carbonation; (Chizmeshya et al., 2007); concurrent grinding and disintegration methods; (Rashid et al., 2021)).

5.3. Opportunities for geochemical CDR within industry

Industrial by-product generation could provide a massive untapped resource for geochemical CDR opportunities, based on the promise of chemically and mineralogically suitable materials, and the huge tonnages of material generation per year (Ahmed et al., 2016, Bobicki et al., 2012; Bullock et al., 2021; Ćwik et al., 2019; Gorai and Jana, 2003). The utilisation of industrial by-products for geochemical CDR purposes may provide a new usage pathway for these materials that would otherwise be of limited or no use to the industrial producer, or materials deemed hazardous to the environment (e.g., carbonation of red muds may mitigate against leaching effects; (Renforth, 2012)). Since most wastes are produced on-site at mines, power plants, refineries, smelters, etc., there are opportunities to apply geochemical CDR methods on-site (or site-adjacent), making the most efficient use of available sources for land space, transport, storage, and reaction acceleration. *Ex-situ* geochemical CDR methods, where the material is moved from its place of origin and typically crushed up or processed to some degree, may comprise aqueous or dry reaction settings above the surface or in the sub-surface, with an engineered approach implemented to accelerate reactions deliberately (with associated additional costs).

While cation release and W_r of some industrial by-products show similar promise to rocks and minerals utilised in geochemical CDR studies and pilot schemes, there is still a need to speed up reactions to achieve meaningful or near-complete dissolution on human-relevant timescales of decades or faster, while additional financial costs and energy penalties require assessement to determine the viability of such acceleration schemes. The experimental procedure of this study utilised concentrated CO_2 in a reactor-style system, which acts to lower pH and promote dissolution at rates greater than that which may be achieved under ambient CO_2 conditions (e.g., atmospheric conditions), whilst also providing CO_2 for bicarbonate and carbonate production. This underscores the potentially crucial role that any CO_2 point source might have in expediting reactions for *ex-situ* geochemical CDR, but realising this potential would likely involve the need for additional facilities dedicated to capturing and concentrating the gas from flue emissions. At industrial centres reliant upon fossil-fuel intensive operations (e.g., smelter and refining activities, cement production, coal-fired power plants), CO_2 or CO_2-rich gas streams may be generated (e.g., by electrolytic and anode production processes). If CO_2 can be captured or enriched from flue gases, this could be utilised in any contained reactor system setting for geochemical CDR. Similarly, any on-site DAC scheme could also provide enriched CO_2 for reactions with industrial by-products, with consideration that needs to be given to additional energy penalties and costs. Enriched CO_2 would help to speed up reactions by ensuring CO_2 supply is not limited for alkalinity and carbonate generation, whilst also creating an acidic environment to speed up the dissolution of targetable minerals (Delerce et al., 2023; Harrison et al., 2013; Pokrovsky and Schott, 2000; Reddy et al., 2009; Reynolds et al., 2014).

W_r may also be increased through harnessing heat potential at industrial sites for increased temperature reactions (Assima et al., 2014; Delerce et al., 2023), though such excess heat at sites is seldom exploited for secondary usage (Fleiter et al., 2020). Taking advantage of hotter climates may also provide a means of increasing reactions for some global localities (Andrews and Taylor, 2019; Bullock et al., 2023a; Edwards et al., 2017; Khudhur et al., 2022; Pogge von Strandmann et al., 2022), relevant for *ex-situ* geochemical CDR possibilities that may exist in some of the source locations of samples used in this study (e.g., samples from Spain, Australia, United States). This is particularly relevant to any open scheme aimed at spreading materials across croplands, coastland, forest, or other suitable areas of extensive land (including land available on industrial sites), whereby SSA exposure to the atmosphere is maximised (i.e., enhanced weathering approaches; (Beerling et al., 2020Meysman and Montserrat, 2017; Montserrat et al., 2017; Schuiling and Krijgsman, 2006; Taylor et al., 2016)).

Besides locality-specific approaches, CDR strategies that could be targeted by industry are also dependant upon the starting mineralogical compositions of the materials. Several samples studied here comprise modal mineralogies that may not contain high amounts of silicates, and may therefore limit the CDR approaches that could be pursued (i.e., alkalinity generation without subsequent carbonate precipitation on human-relevant timescales). Red muds, such as those utilised in this study, have the potential to remove CO_2 under ambient conditions under the right conditions that optimise the hyperalkalinity of the solutions whilst preventing excess alkalinity loss that may occur during treatment with seawater (Khudhur et al., 2022; Renforth et al., 2012; Si et al., 2003). Calcite and carbonate-rich materials, such as the marble quarry cuttings studied here, can also provide opportunities for alkalinity generation and OAE, though some of these approaches require (potentially spatially, financially, and energetically intensive) calcination methods, restricted to CO_2-enriched waters (e.g., for seawater usage) in a reactor-type system (Caldeira and Rau, 2000; Darton et al., 2022; Xing et al., 2022). Recent work by Renforth et al. (2022) demonstrated that some hydrated carbonate minerals, such as ikaite ($CaCO_3{\cdot}6H_2O$), could be specifically created from calcite-bearing carbonate materials for geochemical CDR purposes, with sufficient stability sustained to target OAE approaches.

Borax samples also indicate a high alkalinity production potential, with notably high increases in pH and alkalinity indicators, as well as Na and Ca cation release, and comparatively fast Si- and Ca-derived W_r, compared to the rest of the sample set. This is despite the borax tailings hosting comparatively lower concentrations of CaO and MgO than Ca-Mg-rich, but slower reacting, silicate-hosting materials. Boron (B) poses a potential environmental risk to water supply (World Health Organization, 2017). Therefore, carbonating materials, and simultaneously incorporating B into secondary carbonate precipitates, may be a necessary risk mitigation strategy. Incorporation of B into calcite, aragonite, and vaterite ($CaCO_3$ polymorph) is possible through adsorption-precipitation processes (Kobayashi et al., 2020; Wang et al., 2018; Xiao et al., 2008), though significant B incorporation may only be possible under high pH (8–12) conditions (Kobayashi et al., 2020). Furthermore, excess B in the solution may inhibit calcite crystal growth from the less thermodynamically stable vaterite. As borax tailings may react with CO_2 to form bicarbonates and carbonates of limited stability under low temperature conditions (forming Na-bicarbonates or Na-carbonates, and boric acid, akin to reaction mechanisms of related Na-metaborate compounds with CO_2; (Uysal et al., 2017)), the use of

such materials in CDR strategies may be limited to processes that store products in specific settings (e.g., pH, temperature, and pressure-controlled systems, thus limiting upscale potential), or for use as additives or as a mixture material with other potential feedstocks to increase pH and initiate carbonate precipitation. As a consequence, any geochemical CDR management with borax tailings would need more careful consideration, potentially requiring closed system reactors or similar setups to operate safely and effectively. Such approaches have been considered, including the production of sodic-boric carbonate by means of reacting CO_2 with diluted Na-borate solvents under high-pressure and temperature reactor conditions (Yilmaz et al., 2009; Yücel, 1973).

Approaches to implementing geochemical CDR methods by relevant industrial sectors under current legislation and wider scientific (and public) perception would ultimately reap the benefits in several years when CDR can be effectively measured, reported, and verified (Measurement, Reporting, and Verification; MRV) as part of either an enforced MRV framework or by internal or widely recognised protocols. Though such MRV protocols are not yet in place, and carbon crediting is not implemented for geochemical CDR beyond voluntary markets, there is an increasing appeal from industry players (e.g., funders and incubators in developing CDR technologies) to fill the gaps that exist in CDR knowledge, MRV, and carbon offsetting (e.g., carbon removal knowledge gaps and MRV framework development by CarbonPlan and Frontier; (Arcusa and Sprenkle-Hyppolite, 2022; Chay et al., 2022; Kracke et al., 2022). Furthermore, there is also scope for CDR strategies that can enhance metal recovery, making CDR implementation efforts more economically feasible, with a lower risk to industrial operators (Hamilton et al., 2018, 2020; Khan et al., 2021; Wang and Dreisinger, 2022; Wang et al., 2021, 2023; Wilson and Hamilton, 2022). By evaluating material availability and reactivity, location, site conditions and reaction acceleration sources, and by conducting thorough techno-economic, co-benefit, and environmental assessments, a site or company can lead in the growing operational carbon removal sector. As certification and carbon crediting become more prevalent throughout the industry, this proactive approach could prove beneficial.

6. Conclusions

The range of industrial by-product samples investigated for their geochemical CDR suitability in this study show variable cation release and surface area-normalised dissolution rates that span several magnitudes. High Ca and Mg release into CO_2-saturated solutions, favouring alkalinity production, has been generally observed in samples associated with dunite mine tailings, kimberlite tailings, ilmenite tailings, and marble quarry cuttings. These samples contain minerals such as brucite, portlandite, saponite, olivine (forsterite), serpentine (chrysotile and lizardite), and carbonates (calcite and dolomite), acting as the main cation sources, though dissolution of carbonates counteracts CDR if subsequent carbonate precipitation occurs. In addition to these high cation releasing samples, borax tailings, fly ashes, and red mud samples show high Si-derived dissolution rates, while fluorite tailings show high Ca-derived dissolution rates, and Ni sulphides show high Mg-derived rates. The achieved rates, which were generally one magnitude slower for geometric surface area-normalised methods than for BET-normalised, are comparable to rates determined for rocks typically targeted for CDR purposes, such as basalt and gabbro.

The fastest dissolution rates of this study (~−11 to −12 log (mol/cm^2/s)) were achieved under more acidic (CO_2-saturated, pH ~3–4 at the start of the experiment, coupled with the highest fraction of finer grained materials present during experimentation) solution conditions, suggesting if sustained acidic conditions, high CO_2 saturation or other means of reaction acceleration can be implemented (e.g., higher temperatures, microbial activity), faster rates can be achieved and prolonged (providing pH eventually rises above ~5.2 to permit alkalinity production from carbonic acids). Sample loss, increases in TIC content, post-experimental changes to modal mineralogies, and aqueous geochemical modelling results suggest that secondary precipitation of a range of carbonates (of variable stability and composition) may occur in ilmenite, borax, Ni sulphide, kimberlite, and dunite samples, indicating that mineral carbonation, in addition to alkalinity generation, may be a usable strategy for geochemical CDR of certain industrial by-products, albeit at a slow rate, under ambient temperature conditions, and in mildly acidic to neutral (pH ~5–7) solutions.

Observations suggest opportunities to explore geochemical CDR strategies with a wide range of industrial by-products, particularly for *ex-situ* strategies that effectively use the voluminous, fine-grained (where already crushed) materials produced in global operations. Furthermore, harvesting on-site or site-proximal sources of reaction accelerants such as heat waste, favourable climates, CO_2-concentrated gases, microorganisms that can thrive in such environments, and available water sources can potentially deliver meaningful CDR on human-relevant timescales. There may also be possible secondary benefits to operators using materials typically considered unwanted or hazardous. Experimental investigations that focus on the geochemical CDR potential of specific materials, sites, and industries, on top of meaningful techno-economic and life cycle assessments, may reap potential environmental and economic benefits in the future.

CRediT authorship contribution statement

Liam A. Bullock: Conceptualization, Methodology, Formal analysis, Investigation, Data curation, Writing – original draft, Visualization, Funding acquisition. **Jose-Luis Fernandez-Turiel:** Methodology, Validation, Formal analysis, Investigation, Writing – review & editing, Visualization, Funding acquisition. **David Benavente:** Methodology, Validation, Formal analysis, Resources, Data curation, Writing – review & editing.

Declaration of Competing Interest

The authors declare that they have no known competing financial interests or personal relationships that could have appeared to influence the work reported in this paper.

Data availability

Data are available through supplementary material and via CSIC repository.

Acknowledgeents

LB and JLFT are funded under H2020-EU.1.3.2. (DETAILS Project, grant agreement ID: 101018312). The authors wish to thank Rio Tinto Group, Pasek Minerales, Atalaya Mining, Atlantic Copper, Minersa Group, and Ring of Fire Metals for their sample provision and project support. The authors wish to thank Marta Rejas Alejos, Soledad Álvarez Pousa, and Jordi Ibáñez Insa (GEO3BCN, CSIC), Rafel Prohens (University of Barcelona), Fiona Keay and Andrew Hobson (University of Leeds) for their technical assistance. The authors appreciate the comments of the anonymous reviewers, and the editorial work of Peter Psarras, that helped to improve the manuscript.

Supplementary materials

Supplementary material associated with this article can be found, in the online version, at doi:10.1016/j.ijggc.2023.103990.

References

Ahmed, S., Saurikhia, A., Haleem, A., Gangopadhyay, S., 2016. Geographical spread of fly ash generation and residual potential for its utilization in India. Int. J. Innov. Res. Rev. 4 (1), 8–19.

Amann, T., Hartmann, J., 2022. Carbon accounting for enhanced weathering. Front. Clim. 4, 849948.

Amponsah-Dacosta, M., 2017. Mineralogical Characterization of South African Mine Tailings With Aim of Evaluating Their Potential For the Purposes of Mineral carbonation. Masters' Thesis. University of Cape Town.

Andrews, M.G., Taylor, L.L., 2019. Combating climate change through enhanced weathering of agricultural soils. Elements 15 (4), 253–258.

Arcusa, S., Sprenkle-Hyppolite, S., 2022. Snapshot of the Carbon Dioxide Removal certification and standards ecosystem (2021–2022). Clim. Policy 22 (9–10), 1319–1332.

Arvidson, R.S., Mackenzie, F.T., 1997. Tentative kinetic model for dolomite precipitation rate and its applications to dolomite dissolution. Aquatic Geochem. 2, 273–398.

Assima, G.P., Larachi, F., Molson, J., Beaudoin, G., 2014. Emulation of ambient carbon dioxide diffusion and carbonation within nickel mining residues. Miner. Eng. 59, 39–44.

Béarat, H., McKelvy, M.J., Chizmeshya, A.V., Gormley, D., Nunez, R., Carpenter, R.W., Squires, K., Wolf, G.H., 2006. Carbon sequestration via aqueous olivine mineral carbonation: role of passivating layer formation. Environ. Sci. Technol. 40 (15), 4802–4808.

Baker, P.A., Cross, S.L., Burns, S.J., Mottl, M.J., Davis, E.E., Fisher, A.T., Slack, J.F., 1994. Geochemistry of carbonate nodules and cements and implications for hydrothermal circulation, Middle Valley, Juan de Fuca Ridge. In: Proceeding of the Ocean Drilling Program, 139, pp. 313–328. Scientific Results.

Banerjee, A., 2016. Estimation of dolomite formation: dolomite precipitation and dolomitization. J. Geol. Soc. India 87, 561–572.

Baragaño, D., Forján, R., Menéndez Aguado, J.M., Covián Martino, M., Díaz García, P., Martínez Rubio, J., Álvarez Rueda, J.J., R. Gallego, J.L., 2019. Reuse of dunite mining waste and subproducts for the stabilization of metal (oid) s in polluted soils. Minerals 9 (8), 481.

Beerling, D.J., Kantzas, E.P., Lomas, M.R., Wade, P., Eufrasio, R.M., Renforth, P., Sarkar, B., Andrews, M.G., James, R.H., Pearce, C.R., Mercure, J.F., 2020. Potential for large-scale CO_2 removal via enhanced rock weathering with croplands. Nature 583 (7815), 242–248.

Benavente, D., Pla, C., Valdes-Abellan, J., Cremades-Alted, S., 2020. Remediation by waste marble powder and lime of jarosite-rich sediments from portman bay (Spain). Environ. Pollut. 264, 114786.

Bobicki, E.R., Liu, Q., Xu, Z., Zeng, H., 2012. Carbon capture and storage using alkaline industrial wastes. Prog. Energy Combust. Sci. 38 (2), 302–320.

Bodénan, F., Bourgeois, F., Petiot, C., Augé, T., Bonfils, B., Julcour-Lebigue, C., et al., 2014. *Ex situ* mineral carbonation for CO_2 mitigation: evaluation of mining waste resources, aqueous carbonation processability and life cycle assessment (Carmex project). Miner. Eng. 59, 52–63.

Bonenfant, D., Kharoune, L., Sauvé, S., Hausler, R., Niquette, P., Mimeault, M., Kharoune, M., 2008. CO_2 sequestration by aqueous red mud carbonation at ambient pressure and temperature. Ind. Eng. Chem. Res. 47 (20), 7617–7622.

Bouillon, S., Yambele, A., Gillikin, D.P., Teodoru, C., Darchambeau, F., Lambert, T., et al., 2014. Contrasting biogeochemical characteristics of the Oubangui River and tributaries (Congo River basin). Sci. Rep. 4, 5402.

Brantley, S.L., Mellott, N.P., 2000. Surface area and porosity of primary silicate minerals. Am. Mineral. 85 (11–12), 1767–1783.

Brunauer, S., Emmett, P.H., Teller, E., 1938. Adsorption of gases in multimolecular layers. J. Am. Chem. Soc. 60 (2), 309–319.

Bullock, L.A., Parnell, J., Perez, M., Armstrong, J.G., 2019. Coal mining-derived ochres in the UK: a potential selenium trap. Geol. Today 35 (4), 140–145.

Bullock, L.A., James, R.H., Matter, J., Renforth, P., Teagle, D.A.H., 2021. Global carbon dioxide removal potential of waste materials from metal and diamond mining. Front. Clim. 3, 694175.

Bullock, L.A., Yang, A., Darton, R., 2022. Kinetics-informed global assessment of mine tailings for CO_2 removal. Sci. Total Environ. 808, 152111.

Bullock, L.A., Alcalde, J., Tornos, F., Fernandez-Turel, J.L., 2023a. Geochemical carbon dioxide removal potential of Spain. Sci. Total Environ. 867, 161287.

Bullock, L.A., Nkosi, Z., Vele, M., Amponsah-Dacosta, M., 2023b. Catalogue of South African mine tailings for geochemical carbon dioxide removal purposes. Int. J. Greenh. Gas Con. 124, 103844.

Caballero, R., García-Arias, M., Rubio, L., Corretgé, L.G., 2009. Dunite-A cost effective raw material in basic refractory mixes for Steel making. In: Proceedings of the 52nd International Colloquium on Refractories. Germany, pp. 23–24. EUROGRESS, Aachen.

Caldeira, K., Rau, G.H., 2000. Accelerating carbonate dissolution to sequester carbon dioxide in the ocean: geochemical implications. Geophys. Res. Lett. 27 (2), 225–228.

Campbell, J.S., Foteinis, S., Furey, V., Hawrot, O., Pike, D., Aeschlimann, S., Maesano, C. N., Reginato, P.L., Goodwin, D.R., Looger, L.L., Boyden, E.S., Renforth, P., 2022. Geochemical negative emissions technologies: part I. Rev. Front. Clim. 4, 133.

Caserini, S., Cappello, G., Righi, D., Raos, G., Campo, F., De Marco, S., Renforth, P., Varliero, S., Grosso, M., 2021. Buffered accelerated weathering of limestone for storing CO_2: chemical background. Int. J. Greenh. Gas Con. 112, 103517.

Chakrabarti, G., Shome, D., Kumar, S., Armstrong-Altrin, J.S., Sial, A.N., 2011. Carbon and oxygen isotopic variations in stromatolitic dolomites of Palaeoproterozoic Vempalle Formation, Cuddapah Basin, India. Carbonate Evaporite 26 (2), 181–191.

Chay, F., Klitzke, J., Hausfather, Z., Martin, K., Freeman, J., Cullenward, D., 2022. Verification confidence levels for carbon dioxide removal. CarbonPlan. https://carbonplan.org/research/cdr-verification-explainer.

Chizmeshya, A.V., McKelvy, M.J., Squires, K., Carpenter, R.W., Béarat, H., 2007. A Novel Approach to Mineral carbonation: Enhancing carbonation While Avoiding Mineral Pretreatment Process Cost. Arizona State Univ., Tempe, AZ (United States).

Colman, S.M., 1981. Rock-weathering rates as functions of time. Quat. Res. 15 (3), 250–264.

Compton, J.S., 1988. Degree of supersaturation and precipitation of organogenic dolomite. Geology 16 (4), 318–321.

Crovisier, J.L., Honnorez, J., Eberhart, J.P., 1987. Dissolution of basaltic glass in seawater: mechanism and rate. Geochim. Cosmochim. Acta 51 (11), 2977–2990.

Curtis, R.E., Evans, G., Kinsman, D.J.J., Shearman, D.J., 1963. Association of dolomite and anhydrite in the recent sediments of the Persian Gulf. Nature 197 (4868), 679–680.

Ćwik, A., Casanova, I., Rausis, K., Zarębska, K., 2019. Utilization of high-calcium fly ashes through mineral carbonation: the cases for Greece, Poland and Spain. J. CO_2 Util 32, 155–162.

Cygan, R.T., Romanov, V.N., Myshakin, E.M., 2012. Molecular simulation of carbon dioxide capture by montmorillonite using an accurate and flexible force field. J. Phys. Chem. C 116 (24), 13079–13091.

Darton, R.C., Yang, A., Xing, L., Bullock, L., 2022. Carbon Dioxide Removal from the atmosphere by weathering minerals in a gas-liquid-solid contactor. In: Proceeding of the 12th International Conference Distillation & Absorption, p. 1202.

Das, S.K., 2015. Quantitative mineralogical characterization of chrome ore beneficiation plant tailing and its beneficiated products. Int. J. Miner. Metall. Mater. 22, 335–345.

Declercq, J., Bowell, R., Brough, C., Barnes, A., Griffiths, R., 2023. Role of Mg gangue minerals in natural analogue CO_2 sequestration. Econ. Geol. 118 (3), 675–688.

Delerce, S., Bénézeth, P., Schott, J., Oelkers, E.H., 2023. The dissolution rates of naturally altered basalts at pH 3 and 120°C: implications for the *in-situ* mineralization of CO_2 injected into the subsurface. Chem. Geol. 621, 121353.

Demadis, K.D., Mavredaki, E., 2005. Green additives to enhance silica dissolution during water treatment. Environ. Chem. Lett. 3, 127–131.

Dichicco, M.C., Laurita, S., Paternoster, M., Rizzo, G., Sinisi, R., Mongelli, G., 2015. Serpentinite carbonation for CO_2 sequestration in the southern apennines: preliminary study. Energy Procedia 76, 477–486.

Dietzen, C., Rosing, M.T., 2023. Quantification of CO_2 uptake by enhanced weathering of silicate minerals applied to acidic soils. Int. J. Greenh. Gas Con. 125, 103872.

Ebrahimi, A., Saffari, M., Hong, Y., Milani, D., Montoya, A., Valix, M., Minett, A., Abbas, A., 2018. Mineral sequestration of CO_2 using saprolite mine tailings in the presence of alkaline industrial wastes. J. Clean. Prod. 188, 686–697.

Edwards, D.P., Lim, F., James, R.H., Pearce, C.R., Scholes, J., Freckleton, R.P., Beerling, D.J., 2017. Climate change mitigation: potential benefits and pitfalls of enhanced rock weathering in tropical agriculture. Biol. Lett. 13 (4), 20160715.

Eick, M.J., Grossl, P.R., Golden, D.C., Sparks, D.L., Ming, D.W., 1996. Dissolution of a lunar basalt simulant as affected by pH and organic anions. Geoderma 74 (1–2), 139–160.

European Commission, 2009. Reference document on best available techniques for management of tailings and waste-rock in mining activities. January 2009 EU Report. Available online. http://eippcb.jrc.ec.europa.eu/.

Fleiter, T., Manz, P., Neuwirth, M., Mildner, F., Persson, U., Kermeli, K., Crijns-Graus, W., Rutten, C., 2020. Documentation on excess heat potentials of industrial sites including open data file with selected potentials. Horizon, 846463, 2020 sEEnergies Deliverable, LC-SC3-EE-14-2018-2019-2020.

Foteinis, S., Andresen, J., Campo, F., Caserini, S., Renforth, P., 2022. Life cycle assessment of ocean liming for carbon dioxide removal from the atmosphere. J. Clean. Prod. 370, 133309.

Gautier, Q., Bénézeth, P., Mavromatis, V., Schott, J., 2014. Hydromagnesite solubility product and growth kinetics in aqueous solution from 25 to 75°C. Geochim. Cosmochim. Acta 138, 1–20.

Giammar, D.E., Bruant, R.G., Peters, C.A., 2005. Forsterite dissolution and magnesite precipitation at conditions relevant for deep saline aquifer storage and sequestration of carbon dioxide. Chem. Geol. 217, 257–276.

Giampouras, E., 2020. Magnesium and Calcium Carbonate Precipitation in Serpentinite-Hosted Alkaline environments: Natural and Experimental Constraints. Universidad de Granada. PhD thesis.

Gislason, S.R., Oelkers, E.H., 2003. Mechanism, rates, and consequences of basaltic glass dissolution: II. An experimental study of the dissolution rates of basaltic glass as a function of pH and temperature. Geochim. Cosmochim. Acta 67 (20), 3817–3832.

Gorai, B., Jana, R.K., 2003. Characteristics and utilisation of copper slag—A review. Resour. Conserv. Recycl. 39 (4), 299–313.

Gudbrandsson, S., Wolff-Boenisch, D., Gislason, S.R., Oelkers, E.H., 2011. An experimental study of crystalline basalt dissolution from 2≤ pH≤ 11 and temperatures from 5 to 75 C. Geochim. Cosmochim. Acta 75 (19), 5496–5509.

Guo, D., Thee, H., da Silva, G., Chen, J., Fei, W., Kentish, S., et al., 2011. Borate-catalyzed carbon dioxide hydration via the carbonic anhydrase mechanism. Environ. Sci. Technol. 45 (11), 4802–4807.

Gysi, A.P., Stefánsson, A., 2012. CO_2-water–basalt interaction. Low temperature experiments and implications for CO_2 sequestration into basalts. Geochim. Cosmochim. Acta 81, 129–152.

Hänchen, M., Prigiobbe, V., Baciocchi, R., Mazzotti, M., 2008. Precipitation in the Mg-carbonate system - effects of temperature and CO_2 pressure. Chem. Eng. Sci. 63, 1012–1028.

Hagens, M., Hartmann, J., Vicca, S., Beerling, D., 2023. Enhanced weathering and synergistic combinations with other CDR methods. Front. Clim. 5, 1244396.

Hamilton, J.L., Wilson, S.A., Morgan, B., Turvey, C.C., Paterson, D.J., Jowitt, S.M., McCutcheon, J., Southam, G., 2018. Fate of transition metals during passive carbonation of ultramafic mine tailings via air capture with potential for metal resource recovery. Int. J. Greenh. Gas Con. 71, 155–167.

Hamilton, J.L., Wilson, S.A., Morgan, B., Harrison, A.L., Turvey, C.C., Paterson, D.J., Dipple, G.M., Southam, G., 2020. Accelerating mineral carbonation in ultramafic mine tailings via direct CO_2 reaction and heap leaching with potential for base metal enrichment and recovery. Econ. Geol. 115 (2), 303–323.

Hangx, S.J.T., Spiers, C.J., 2009. Coastal spreading of olivine to control atmospheric CO_2 concentrations: a critical analysis of viability. Int. J. Greenh. Gas Con. 3, 757–767.

Harrison, A.L., Power, I.M., Dipple, G.M., 2013. Accelerated carbonation of brucite in mine tailings for carbon sequestration. Environ. Sci. Technol. 47, 126–134.

Harrison, A.L., Dipple, G.M., Power, I.M., Mayer, K.U., 2015. Influence of surface passivation and water content on mineral reactions in unsaturated porous media: implications for brucite carbonation and CO_2 sequestration. Geochim. Cosmochim. Acta 148, 477–495.

Harvey, L.D.D., 2008. Mitigating the atmospheric CO_2 increase and ocean acidification by adding limestone powder to upwelling regions. J. Geophys. Res. Oceans 113 (C4).

Hitch, M., Ballantyne, S.M., Hindle, S.R., 2010. Revaluing mine waste rock for carbon capture and storage. Int. J. Min. Reclamat. Environ. 24, 64–79.

Hopkinson, L., Kristova, P., Rutt, K., Cressey, G., 2012. Phase transitions in the system MgO–CO_2–H_2O during CO_2 degassing of Mg-bearing solutions. Geochim. Cosmochim. Acta 76, 1–13.

Hostetler, P.B., Coleman, R.G., Mumpton, F.A., Evan, B.W., 1966. Brucite in alpine serpentinites. Am. Mineral. 51 (75), 98.

House, K.Z., House, C.H., Schrag, D.P., Aziz, M.J., 2007. Electrochemical acceleration of chemical weathering as an energetically feasible approach to mitigating anthropogenic climate change. Environ. Sci. Technol. 41 (24), 8464–8470.

Hu, L., Wu, H., Zhang, L., Zhang, P., 2017. Geotechnical properties of mine tailings. J. Mater. Civ. Eng. 29 (2), 04016220.

Huijgen, W.J., Witkamp, G.J., Comans, R.N., 2005. Mineral CO_2 sequestration by steel slag carbonation. Environ. Sci. Technol. 39 (24), 9676–9682.

IPCC (Intergovernmental Panel on Climate Change), 2018. Climate Change 2013: Global Warming of 1.5 °C. IPCC, Geneva.

IPCC (Intergovernmental Panel on Climate Change), 2019. IPCC Special Report On the Ocean and Cryosphere in a Changing Climate. IPCC, Geneva.

Janssens, I.A., Roobroeck, D., Sardans, J., Obersteiner, M., Peñuelas, J., Richter, A., Smith, P., Verbruggen, E., Vicca, S., 2022. Negative erosion and negative emissions: combining multiple land-based carbon dioxide removal techniques to rebuild fertile topsoils and enhance food production. Front. Clim. 4, 928403.

Jones, G., Joshi, G., Clark, M.W., McConchie, D.M., 2006. Carbon capture and the aluminium industry: preliminary studies. Environ. Chem. 3 (4), 297–303.

Kısakürek, B., Widdowson, M., James, R.H., 2004. Behaviour of Li isotopes during continental weathering: the Bidar laterite profile, India. Chem. Geol. 212 (1–2), 27–44.

Kandji, E.H.B., Plante, B., Bussière, B., Beaudoin, G., Dupont, P.P., 2017. Geochemical behavior of ultramafic waste rocks with carbon sequestration potential: a case study of the dumont nickel project, Amos, Québec. Environ. Sci. Pollut. Res. 24 (12), 11734–11751.

Kelemen, P.B., Matter, J., Streit, E.E., Rudge, J.F., Curry, W.B., Blusztajn, J., 2011. Rates and mechanisms of mineral carbonation in peridotite: natural processes and recipes for enhanced, *in situ* CO_2 capture and storage. Annu. Rev. Earth Planet. Sci. 39, 545–576.

Kelemen, P.B., McQueen, N., Wilcox, J., Renforth, P., Dipple, G., Vankeuren, A.P., 2020. Engineered carbon mineralization in ultramafic rocks for CO_2 removal from air: review and new insights. Chem. Geol. 550, 119628.

Khan, S., Wani, O.B., Shoaib, M., Forster, J., Sodhi, R.N., Boucher, D., Bobicki, E.R., 2021. Mineral carbonation for serpentine mitigation in nickel processing: a step towards industrial carbon capture and storage. Faraday Discuss. 230, 172–186.

Kheshgi, H.S., 1995. Sequestering atmospheric carbon dioxide by increasing ocean alkalinity. Energy 20, 915–922.

Khudhur, F.W., MacDonald, J.M., Macente, A., Daly, L., 2022. The utilization of alkaline wastes in passive carbon capture and sequestration: promises, challenges and environmental aspects. Sci. Total Environ., 153553

Kirchner, J.S., Lettmann, K.A., Schnetger, B., Wolff, J.O., Brumsack, H.J., 2020. Carbon capture via accelerated weathering of limestone: modeling local impacts on the carbonate chemistry of the southern North Sea. Int. J. Greenh. Gas Con. 92, 102855.

Kloprogge, T., Martens, W., Nothdurft, L., Duong, L., Webb, G., 2003. Low temperature synthesis and characterization of nesquehonite. J. Mater. Sci 22, 825–829.

Kobayashi, K., Hashimoto, Y., Wang, S.L., 2020. Boron incorporation into precipitated calcium carbonates affected by aqueous pH and boron concentration. J. Hazard. Mater. 383, 121183.

Kracke, F., Klitze, J., Ransohoff, N., 2022. Carbon Removal Knowledge Gaps. Frontier Climate. https://frontierclimate.com/writing/cdr-gap-database.

Kremer, D., Wotruba, H., 2020. Separation of products from mineral sequestration of CO_2 with primary and secondary raw materials. Minerals 10 (12), 1098.

Kremer, D., Etzold, S., Boldt, J., Blaum, P., Hahn, K.M., Wotruba, H., Telle, R., et al., 2019. Geological mapping and characterization of possible primary input materials for the mineral sequestration of carbon dioxide in Europe. Minerals 9, 485.

Kremer, D., Dertmann, C., Etzold, S., Telle, R., Friedrich, B., Wotruba, H., 2022. *Ex-situ* mineral carbonation – A parameter study on carbon mineralisation in an autoclave as part of a large-scale utilisation process. J. CO_2 Util. 58, 101928.

Kursun, I., Ozdemir, O., Eskibalci, F., Hacifazlioglu, H., Terzi, M., 2017. Dissolution of lead from lead-zinc tailings with nitric acid. In: Proceedings of the XVII Balkan Mineral Processing Congress, XVII BMPC. Tiran-Albania, pp. 493–498.

Lacinska, A.M., Styles, M.T., Bateman, K., Hall, M., Brown, P.D., 2017. An experimental study of the carbonation of serpentinite and partially serpentinised peridotites. Front. Earth Sci. 5, 37.

Land, L.S., 1973. Holocene meteoric dolomitization of Pleistocene limestones, North Jamaica. Sedimentology 20 (3), 411–424.

Langmuir, D., 1997. Aqueous Environmental Geochemistry. Prentice Hall, Upper Saddle River, NJ, p. 600.

Li, J., Hitch, M., Power, I.M., Pan, Y., 2018. Integrated mineral carbonation of ultramafic mine deposits—A review. Minerals 8, 147.

Liittge, A., Arvidson, R.S., Brantley, K., 2008. The Mineral–Water Interface. White Kinetics of Water-Rock Interaction 73–107, 2008.

Lippmann, F., 1973. Sedimentary Carbonate Minerals. Springer-Verlag, New York, NY, p. 228.

Liu, Y., Ali, A., Su, J.F., Li, K., Hu, R.Z., Wang, Z., 2023. Microbial-induced calcium carbonate precipitation: influencing factors, nucleation pathways, and application in waste water remediation. Sci. Total Environ., 160439

Lu, X., Wang, X., Dipple, G.M., 2023. Characterizing reactivity of ultramafic minerals and tailings in british columbia for carbon capture and storage. Geoscience BC Summary of Activities 2022: Minerals, Geoscience BC, Report 2023-01, 45–54. Available online: https://cdn.geosciencebc.com/project_data/GBCReport2023-01/Sch_Lu_MineralsSoA2022.pdf.

Machel, H.G., 2004. Concepts and models of dolomitization: a critical reappraisal. In: C. J.R. Braithwaite, G. Rizzi, and G. Darke, (Eds.), The Geometry and Petrogenesis of Dolomite Hydrocarbon Reservoirs: Geol. Soc. London Spec. Publ. 235, 7–63.

Magenheim, A.J., Gieskes, J.M., 1992. Hydrothermal discharge and alteration in near surface sediments from the Guaymas Basin, Gulf of California. Geochim. Cosmochim. Acta 56 (6), 2329–2338.

Marieni, C., Matter, J.M., Teagle, D.A., 2020. Experimental study on mafic rock dissolution rates within CO_2-seawater-rock systems. Geochim. Cosmochim. Acta 272, 259–275.

Martín Ramos, J.D., 2004. XPowder, a software package for powder X-ray diffraction analysis. legal deposit GR, 1001(04).

Matter, J., Stute, M., Snæbjörnsdottir, S.Ó., Oelkers, E.H., Gislason, S.R., Aradottir, E.S., et al., 2016. Rapid carbon mineralization for permanent disposal of anthropogenic carbon dioxide emissions. Science 352 (6291), 1312–1314.

McCutcheon, J., Wilson, S., Southam, G., 2015. Microbially accelerated carbonate mineral precipitation as a strategy for in situ carbon sequestration and rehabilitation of asbestos mine sites. Environ. Sci. Technol. 50 (3), 1419–1427.

McCutcheon, J., Wilson, S.A., Southam, G., 2016. Microbially accelerated carbonate mineral precipitation as a strategy for *in situ* carbon sequestration and rehabilitation of asbestos mine sites. Environ. Sci. Technol. 50, 1419–1427.

McCutcheon, J., Turvey, C., Wilson, S.A., Hamilton, J.L., Southam, G., 2017. Experimental deployment of microbial mineral carbonation at an asbestos mine: potential applications to carbon storage and tailings stabilization. Minerals 7, 191.

McKenzie, J.A., Vasconcelos, C., 2009. Dolomite Mountains and the origin of the dolomite rock of which they mainly consist: historical developments and new perspectives. Sedimentology 56 (1), 205–219.

Mervine, E.M., Wilson, S.A., Power, I.M., Dipple, G.M., Turvey, C.C., Hamilton, J.L., et al., 2018. Potential for offsetting diamond mine carbon emissions through mineral carbonation of processed kimberlite: an assessment of De Beers mine sites in South Africa and Canada. Mineral. Petrol. 112, 755–765.

Meysman, F.J., Montserrat, F., 2017. Negative CO_2 emissions via enhanced silicate weathering in coastal environments. Biol. Lett. 13 (4), 20160905.

Michels, L., Fossum, J.O., Rozynek, Z., Hemmen, H., Rustenberg, K., Sobas, P.A., et al., 2015. Intercalation and retention of carbon dioxide in a smectite clay promoted by interlayer cations. Sci. Rep. 5, 8775.

Montserrat, F., Renforth, P., Hartmann, J., Leermakers, M., Knops, P., Meysman, F.J., 2017. Olivine dissolution in seawater: implications for CO_2 sequestration through enhanced weathering in coastal environments. Environ. Sci. Technol. 51 (7), 3960–3972.

Moras, C.A., Bach, L.T., Cyronak, T., Joannes-Boyau, R., Schulz, K.G., 2022. Ocean alkalinity enhancement–avoiding runaway $CaCO_3$ precipitation during quick and hydrated lime dissolution. Biogeosciences 19 (15), 3537–3557.

Mumpton, F.A., Thompson, C.S., 1967. The stability of brucite in the weathering zone of the New Idria Serpentinite. In: Proceedings of the Fourteenth National Conference on Clays and Clay Minerals. Berkeley, CA, pp. 249–257.

Mustafa, J., Aya, A.H.M., Al-Marzouqi, A.H., El-Naas, M.H., 2020. Simultaneous treatment of reject brine and capture of carbon dioxide: A comprehensive review. Desalination 483, 114386.

National Academies of Sciences, Engineering, and Medicine (NASEM), 2019. Negative Emissions Technologies and Reliable Sequestration: A Research Agenda. The National Academies Press, Washington DC NPR, p. 2021.

Oelkers, E.H., 2001. General kinetic description of multioxide silicate mineral and glass dissolution. Geochim. Cosmochim. Acta 65 (21), 3703–3719.

Oskierski, H.C., 2013. Natural Carbonation of Ultramafic Rocks in the Great Serpentinite Belt, New South Wales. Australia. PhD thesis.

Palandri, J.L., Kharaka, Y.K., 2005. Ferric iron-bearing sediments as a mineral trap for CO_2 sequestration: iron reduction using sulfur-bearing waste gas. Chem. Geol. 217, 351–364.

Parkhurst, D.L., Appelo, C.A.J., 2013. Description of input and examples for PHREEQC version 3—A computer program for speciation, batch-reaction, one-dimensional transport, and inverse geochemical calculations. US Geol. Surv. Tech. Methods 6 (A43), 497.

Paulo, C., Power, I.M., Stubbs, A.R., Wang, B., Zeyen, N., Wilson, S.A., 2021. Evaluating feedstocks for carbon dioxide removal by enhanced rock weathering and CO_2 mineralization. Appl. Geochem. 129, 104955.

Pla, C., Benavente, D., Valdes-Abellan, J., Jodar-Abellan, A., 2021. Recovery of polluted urban stormwater containing heavy metals: laboratory-based experiments with arlita and filtralite. Water 13 (6), 780 (Basel).
Plumlee, G.S., Leach, D.L., Hofstra, A.H., Landis, G.P., Rowan, E.L., Viets, J.G., 1994. Chemical reaction path modelling of ore deposition in Mississippi Valley–Type Pb–Zn deposits of the Ozark region, United-States midcontinent. Econ. Geol. 89 (6), 1361–1383.
Pogge von Strandmann, P.A.E., Burton, K.W., Snæbjörnsdóttir, S.O., Sigfússon, B., Aradóttir, E.S., Gunnarsson, I., et al., 2019. Rapid CO_2 mineralisation into calcite at the CarbFix storage site quantified using calcium isotopes. Nat. Commun. 10, 1983.
Pogge von Strandmann, P.A., Tooley, C., Mulders, J.J., Renforth, P., 2022. The dissolution of olivine added to soil at 4°C: implications for enhanced weathering in cold regions. Front. Clim. 4, 8.
Pokrovsky, O.S., Schott, J., 2000. Kinetics and mechanism of forsterite dissolution at 25°C and pH from 1 to 12. Geochim. Cosmochim. Acta 64, 3313–3325.
Power, I.M., Harrison, A.L., Dipple, G.M., Southam, G., 2013a. Carbon sequestration via carbonic anhydrase facilitated magnesium carbonate precipitation. Int. J. Greenh. Gas Con. 16, 145–155.
Power, I.M., Wilson, S.A., Dipple, G.M., 2013b. Serpentinite carbonation for CO_2 sequestration. Elements 9, 115–121.
Power, I.M., McCutcheon, J., Harrison, A.L., Wilson, S.A., Dipple, G.M., Kelly, S., et al., 2014. Strategizing carbon-neutral mines: a case for pilot projects. Minerals 4, 399–436.
Power, I.M., Harrison, A.L., Dipple, G.M., 2016. Accelerating mineral carbonation using carbonic anhydrase. Environ. Sci. Technol. 50, 2610–2618.
Power, I.M., Harrison, A.L., Dipple, G.M., Wilson, S.A., Barker, S.L.L., Fallon, S.J., 2019. Magnesite formation in playa environments near Atlin, British Columbia. Canada. Geochim. Cosmochim. Acta 255, 1–24.
Power, I.M., Dipple, G.M., Bradshaw, P.M.D., Harrison, A.L., 2020. Prospects for CO_2 mineralization and enhanced weathering of ultramafic mine tailings from the Baptise nickel deposit in British Columbia. Canada. Int. J. Greenh. Gas Con. 94, 102895.
Pronost, J., Beaudoin, G., Tremblay, J., Larachi, F., Duchesne, J., Hébert, R., et al., 2011. Carbon sequestration kinetic and storage capacity of ultramafic mining waste. Environ. Sci. Technol. 45, 9413–9420.
Proulx, C.L., Kilgour, B.W., Francis, A.P., Bouwhuis, R.F., Hill, J.R., 2018. Using a conductivity–alkalinity relationship as a tool to identify surface waters in reference condition across Canada. Water Qual. Res. J. 53, 231–240.
Pullin, H., Bray, A.W., Burke, I.T., Muir, D.D., Sapsford, D.J., Mayes, W.M., Renforth, P., 2019. Atmospheric carbon capture performance of legacy iron and steel waste. Environ. Sci. Technol. 53 (16), 9502–9511.
Rackley, S.A., 2017. Mineral carbonation. Rackley Carbon Capture and Storage, Second Ed. Butterworth-Heinemann, pp. 253–282. https://doi.org/10.1016/B978-0-12-812041-5.00010-6.
Rashid, M.I., Benhelal, E., Farhang, F., Oliver, T.K., Stockenhuber, M., Kennedy, E.M., 2021. Application of concurrent grinding in direct aqueous carbonation of magnesium silicates. J. CO_2 Util. 48, 101516.
Rau, G.H., Caldeira, K., 1999. Enhanced carbonate dissolution: a means of sequestering waste CO_2 as ocean bicarbonate. Energy Convers. Manag. 40 (17), 1803–1813.
Rau, G.H., Knauss, K.G., Langer, W.H., Caldeira, K., 2007. Reducing energy-related CO_2 emissions using accelerated weathering of limestone. Energy 32 (8), 1471–1477.
Rau, G.H., 2008. Electrochemical splitting of calcium carbonate to increase solution alkalinity: implications for mitigation of carbon dioxide and ocean acidity. Environ. Sci. Technol. 42 (23), 8935–8940.
Rausis, K., Ćwik, A., Casanova, I., Zarębska, K., 2021. Carbonation of high-Ca fly ashes under flue gas conditions: implications for their valorization in the construction industry. Crystals 11 (11), 1314.
Reddy, K.J., Argyle, M.D., Viswatej, A., Taylor, D.T., 2009. A novel method to capture and store flue gas carbon dioxide (CO_2): accelerated mineral carbonation. IOP Conf. Ser. Earth Environ. Sci., 6, 17. IOP Publishing.
Renforth, P., Henderson, G., 2017. Assessing ocean alkalinity for carbon sequestration. Rev. Geophys. 55 (3), 636–674.
Renforth, P., Washbourne, C.L., Taylder, J., Manning, D.A.C., 2011. Silicate production and availability for mineral carbonation. Environ. Sci. Technol. 45 (6), 2035–2041.
Renforth, P., Mayes, W.M., Jarvis, A.P., Burke, I.T., Manning, D.A., Gruiz, K., 2012. Contaminant mobility and carbon sequestration downstream of the Ajka (Hungary) red mud spill: the effects of gypsum dosing. Sci. Total Environ. 421, 253–259.
Renforth, P., Jenkins, B.G., Kruger, T., 2013. Engineering challenges of ocean liming. Energy 60, 442–452.
Renforth, P., Pogge von Strandmann, P.A.E., Henderson, G.M., 2015. The dissolution of olivine added to soil: implications for enhanced weathering. Appl. Geochem. 61, 109–118.
Renforth, P., Baltruschat, S., Peterson, K., Mihailova, B.D., Hartmann, J., 2022. Using ikaite and other hydrated carbonate minerals to increase ocean alkalinity for carbon dioxide removal and environmental remediation. Joule 6 (12), 2674–2679.
Renforth, P., 2012. The potential of enhanced weathering in the UK. Int. J. Greenh. Gas Con. 10, 229–243.
Renforth, P., 2019. The negative emission potential of alkaline materials. Nat. Commun. 10, 1401.
Reynolds, B., Reddy, K.J., Argyle, M.D., 2014. Field application of accelerated mineral carbonation. Minerals 4 (2), 191–207.
Rigopoulos, I., Vasiliades, M.A., Petallidou, K.C., Ioannou, I., Efstathiou, A.M., Kyratsi, T., 2015. A method to enhance the CO_2 storage capacity of pyroxenitic rocks. Greenh. Gas. Sci. Technol. 5, 1–14.
Rizwan, M., Ali, S., Qayyum, M.F., Ibrahim, M., Zia-ur-Rehman, M., Abbas, T., Ok, Y.S., 2016. Mechanisms of biochar-mediated alleviation of toxicity of trace elements in plants: a critical review. Environ. Sci. Pollut. Res. 23, 2230–2248.
Roberts, J.A., Bennett, P.C., Gonzalez, L.A., MacPherson, G.L., Milliken, K.L., 2004. Microbial precipitation of dolomite in methanogenic groundwater. Geology 32 (4), 277–280.
Rodríguez, R.L., Lloret, A., Ledesma, A., Candela, L., 1998. Characterization of mine tailings in the Cuban nickel industry. Sêco e Pinto (Ed.), Environmental Geotechnics: . In: Proceedings of the Third International Congress on Environmental Geotechnics. Balkema, Lisbon, Portugal, pp. 7–11.
Rosen, M.R., Miser, D.E., Starcher, M.A., Warren, J.K., 1989. Formation of dolomite in the Coorong region, South Australia. Geochim. Cosmochim. Acta 53 (3), 661–669.
Ruibal, C., Platas, G., Bills, G.F., 2005. Isolation and characterization of melanized fungi from limestone formations in Mallorca. Mycol. Prog. 4, 23–38.
Ruiz-Agudo, E., Putnis, C.V., Rodriguez-Navarro, C., Putnis, A., 2012. Mechanism of leached layer formation during chemical weathering of silicate minerals. Geology 40 (10), 947–950.
Ruiz-Agudo, E., Putnis, C.V., Putnis, A., 2014. Coupled dissolution and precipitation at mineral–fluid interfaces. Chem. Geol. 383, 132–146.
Sánchez-Román, M., Vasconcelos, C., Schmid, T., Dittrich, M., McKenzie, J.A., Zenobi, R., Rivadeneyra, M.A., 2008. Aerobic microbial dolomite at the nanometer scale: implications for the geologic record. Geology 36 (11), 879–882.
Saldi, G.D., Jordan, G., Schott, J., Oelkers, E.H., 2009. Magnesite growth rates as a function of temperature and saturation state. Geochim. Cosmochim. Acta 73, 5646–5657.
Saldi, G.D., Schott, J., Pokrovsky, O.S., Gautier, Q., Oelkers, E.H., 2012. An experimental study of magnesite precipitation rates at neutral to alkaline conditions and 100–200°C as a function of pH, aqueous solution composition and chemical affinity. Geochim. Cosmochim. Acta 83, 93–109.
Sanjuán, I., Benavente, D., Expósito, E., Montiel, V., 2019. Electrochemical water softening: influence of water composition on the precipitation behaviour. Sep. Purif. Technol. 211, 857–865.
Schuiling, R.D., de Boer, P.L., 2011. Rolling stones; fast weathering of olivine in shallow seas for cost-effective CO_2 capture and mitigation of global warming and ocean acidification. Earth Syst. Dynam. Discuss. 2, 551–568.
Schuiling, R.D., Krijgsman, P., 2006. Enhanced weathering: an effective and cheap tool to sequester CO_2. Clim. Change 74 (1–3), 349–354.
Schulz, K.J., DeYoung Jr, J.H., Seal II, R.R., Bradley, D.C., 2017. Critical mineral resources of the United States—Economic and environmental geology and prospects for future supply. U.S. Geol. Surv. Prof. Pap. 1802-T.
Sechriest, R.E., 1960. Relationship between total alkalinity, conductivity, original pH, and buffer action of natural water. Ohio J. Sci. 60, 303–308.
Si, X., Deng, Z., Xu, Y., 2003. Summarization of extracting scandium from red mud. Jiangxi Nonferrous Met. 17, 28–31.
Srivastava, S., Snellings, R., Nielsen, P., Cool, P., 2022. Insights into CO_2-mineralization using non-ferrous metallurgy slags: cO_2(g)-induced dissolution behavior of copper and lead slags J. Environ. Chem. Eng. 10 (2), 107338.
Stipp, S.L.S., Hansen, M., Kristensen, R., Hochella Jr, M.F., Bennedsen, L., Dideriksen, K., Balic-Zunic, T., Leonard, D., Mathieu, H.J., 2002. Behaviour of Fe-oxides relevant to contaminant uptake in the environment. Chem. Geol. 190 (1–4), 321–337.
Stockmann, G.J., Shirokova, L.S., Pokrovsky, O.S., Bénézeth, P., Bovet, N., Gislason, S.R., Oelkers, E.H., 2012. Does the presence of heterotrophic bacterium Pseudomonas reactans affect basaltic glass dissolution rates? Chem. Geol. 296, 1–18.
Stubbs, A.R., Paulo, C., Power, I.M., Wang, B., Zeyen, N., Wilson, S.A., 2022. Direct measurement of CO_2 drawdown in mine wastes and rock powders: implications for enhanced rock weathering. Int. J. Greenh. Gas Con. 113, 103554.
Swami, R.K., Pundhir, N.K.S., Mathur, S., 2007. Kimberlite tailings: a road construction material. J. Transp. Res. Board 131–134, 1989-2 (1).
Taylor, L.L., Quirk, J., Thorley, R.M., Kharecha, P.A., Hansen, J., Ridgwell, A., Lomas, M. R., Banwart, S.A., Beerling, D.J., 2016. Enhanced weathering strategies for stabilizing climate and averting ocean acidification. Nat. Clim. Change 6 (4), 402–406.
te Pas, E.E.E.M, Comans, R.N.J., Hagens, M., 2023. Can combinations of enhanced weathering and biochar co-benefit crop productivity and soil CO_2 sequestration? Goldschmidt2023 abstract, Lyon, France.
ten Berge, H.F.M., van der Meer, H.G., Steenhuizen, J.W., Goedhart, P.W., Knops, P., Verhagen, J., 2012. Olivine weathering in soil, and its effects on growth and nutrient uptake in ryegrass (Lolium perenne L.): a pot experiment. PLoS One 7, e42098.
Tucker, M.E., 1982. Precambrian dolomites: petrographic and isotopic evidence that they differ from Phanerozoic dolomites. Geology 10 (1), 7–12.
United Nations Environment Programme (UNEP), 2022. Emissions Gap Report 2022: The Closing Window — Climate crisis calls for rapid transformation of societies. Nairobi Available online: https://www.unep.org/emissions-gap-report-2022.
Usdowski, E., 1989. Synthesis of dolomite and magnesite at 60°C in the system Ca2+–Mg2+–CO32−–Cl22–H2O. Naturwissenschaften 76, 374–375.
Uysal, D., Dogan, O.M., Uysal, B.Z., 2017. Kinetics of absorption of carbon dioxide into sodium metaborate solution. Int. J. Chem. Kinet. 49 (6), 377–386.
Van Lith, Y., Warthmann, R., Vasconcelos, C., McKenzie, J.A., 2003. Sulphate–reducing bacteria induce low–temperature Ca-dolomite and high Mg-calcite formation. Geobiology 1 (1), 71–79.
Vance, D., Teagle, D.A.H., Foster, G.L., 2009. Variable Quaternary chemical weathering fluxes and imbalances in marine geochemical budgets. Nature 458, 493–496.
Vasconcelos, C., McKenzie, J.A., 1997. Microbial mediation of modern dolomite precipitation and diagenesis under anoxic conditions (Lagoa Vermelha, Rio de Janeiro, Brazil). Jour. Sediment. Res. 67 (3), 378–390.

Vasconcelos, C., McKenzie, J.A., Bernasconi, S., Grujic, D., Tien, A.J., 1995. Microbial mediation as a possible mechanism for natural dolomite formation at low temperatures. Nature 377, 220–222.
Vogeli, J., Reid, D.L., Becker, M., Broadhurst, J., Franzidis, J.P., 2011. Investigation of the potential for mineral carbonation of PGM tailings in South Africa. Miner. Eng. 24, 1348–1356.
Wang, F., Dreisinger, D., 2022. Carbon mineralization with concurrent critical metal recovery from olivine. Proc. Natl. Acad. Sci. U.S.A 119 (32), e2203937119.
Wang, X., Maroto-Valer, M.M., 2011. Dissolution of serpentine using recyclable ammonium salts for CO_2 mineral carbonation. Fuel 90, 1229–1237.
Wang, Y.J., Wei, H.Z., Jiang, S.Y., van de Ven, T.G.M., Ling, B.P., Li, Y.C., Lin, Y.B., Guo, Q., 2018. Mechanism of boron incorporation into calcites and associated isotope fractionation in a steady-state carbonate-seawater system. Appl. Geochem. 98, 221–236.
Wang, X., Ni, W., Li, J., Zhang, S., Hitch, M., Pascual, R., 2019. Carbonation of steel slag and gypsum for building materials and associated reaction mechanisms. Cem. Concr. Res. 125, 105893.
Wang, F., Dreisinger, D., Jarvis, M., Hitchins, T., Trytten, L., 2021. CO_2 mineralization and concurrent utilization for nickel conversion from nickel silicates to nickel sulfides. Chem. Eng. J. 406, 126761.
Wang, X., Lu, X., Turvy, C., Dipple, G.M., Ni, W., 2022. Evaluation of the carbon sequestration potential of steel slag in China based on theoretical and experimental labile Ca. Resour. Conserv. Recycl. 186, 106590.
Wang, F., Dreisinger, D., Xiao, Y., 2023. Accelerated CO_2 mineralization and utilization for selective battery metals recovery from olivine and laterites. J. Clean. Prod. 393, 136345.
Weber, J.N., 1964. Trace element composition of dolostones and dolomites and its bearing on the dolomite problem. Geochim. Cosmochim. Acta 28, 1817–1832.
Wells, A., 1962. Primary dolomitization in Persian Gulf. Nature 194, 274–275.
Wilson, S.A., Hamilton, J.L., 2022. Fizzy ore processing sequesters CO_2 while supplying critical metals. Proc. Natl. Acad. Sci. 119 (39), e2212424119.
Wilson, S.A., Dipple, G.M., Power, I.M., Thom, J.M., Anderson, R.G., Raudsepp, M., et al., 2009a. Carbon dioxide fixation within mine wastes of ultramafic hosted ore deposits: examples from the Clinton Creek and Cassiar chrysotile deposits. Canada. Econ. Geol. 104, 95–112.
Wilson, S.A., Raudsepp, M., Dipple, G.M., 2009b. Quantifying carbon fixation in trace minerals from processed kimberlite: a comparative study of quantitative methods using X-ray powder diffraction data with applications to the Diavik Diamond Mine, Northwest Territories. Canada. Appl. Geochem. 24, 2312–2331.
Wilson, S.A., Dipple, G.M., Power, I.M., Barker, S.L.L., Fallon, S.J., Southam, G., 2011. Subarctic weathering of mineral wastes provides a sink for atmospheric CO_2. Environ. Sci. Technol. 45, 7727–7736.
Wilson, S.A., Harrison, A.L., Dipple, G.M., Power, I.M., Barker, S.L.L., Mayer, K.U., et al., 2014. Offsetting of CO_2 emissions by air capture in mine tailings at the Mount Keith Nickel Mine, Western Australia: rates, controls and prospects for carbon neutral mining. Int. J. Greenh. Gas Con. 25, 121–140.
Wolff-Boenisch, D., Gislason, S.R., Oelkers, E.H., Putnis, C.V., 2004. The dissolution rates of natural glasses as a function of their composition at pH 4 and 10.6, and temperatures from 25 to 74°C. Geochim. Cosmochim. Acta 68 (23), 4843–4858.
World Health Organization, 2017. Guidelines For Drinking-water Quality: Fourth Edition Incorporating the First Addendum. WHO, Geneva.
Xiao, Y., Li, H., Liu, W., Wang, X., Jiang, S., 2008. Boron isotopic fractionation in laboratory inorganic carbonate precipitation: evidence for the incorporation of B $(OH)_3$ into carbonate. Sci. China Ser. D. Earth Sci. 51 (12), 1776–1785.
Xing, L., Pullin, H., Bullock, L.A., Renforth, P., Darton, R.C., Yang, A., 2022. Potential of enhanced weathering of calcite in packed bubble columns with seawater for carbon dioxide removal. Chem. Eng. J. 431, 134096.
Yücel, H., 1973. Production of Boric Acid and Sodium Bicarbonate from Carbonation and Sodium Tetiaborate. Middle East Technical University. Masters' thesis.
Yilmaz, O., Unlu, F., Karakoc, G., Marasliogl u, D., Gokcek, S., Karacay, E., Demirhan, M. H., Cetin, C.E., Iplikcioglu, O., 2009. Production of boric carbonate and sodium bicarbonate from sodium borate solvents. Patent WO2010140989 A, 1, p. 2010.
Zeyen, N., Wang, B., Wilson, S.A., Paulo, C., Stubbs, A.R., Power, I.M., Steele-Maclnnis, M., Lanzirotti, A., Newville, M., Paterson, D.J., Hamilton, J.L., 2022. Cation exchange in smectites as a new approach to mineral carbonation. Front. Clim. 4, 913632.